NASA TECHNICAL MEMORANDUM

NASA TM X-2537

NASA TM X-2537

PERFORMANCE AND CONTROL STUDY OF A LOW-PRESSURE-RATIO TURBOJET ENGINE FOR A DRONE AIRCRAFT

by Kurt Seldner, Lucille C. Geyser, Harold Gold, Darrel Walker, and Gary Burgner

Lewis Research Center
Cleveland, Ohio 44135

NATIONAL AERONAUTICS AND SPACE ADMINISTRATION • WASHINGTON, D. C. • APRIL 1972

1. Report No.	2. Government Accession No.	3. Recipient's Catalog No.
NASA TM X-2537		

4. Title and Subtitle	5. Report Date
PERFORMANCE AND CONTROL STUDY OF A LOW-PRESSURE-RATIO TURBOJET ENGINE FOR A DRONE AIRCRAFT	April 1972
	6. Performing Organization Code

7. Author(s)	8. Performing Organization Report No.
Kurt Seldner, Lucille C. Geyser, Harold Gold, Lewis Research Center; Darrel Walker, and Gary Burgner, Naval Weapons Center, China Lake, California	E-6688
	10. Work Unit No. 132-15
9. Performing Organization Name and Address Lewis Research Center National Aeronautics and Space Administration Cleveland, Ohio 44135	11. Contract or Grant No.
	13. Type of Report and Period Covered Technical Memorandum
12. Sponsoring Agency Name and Address National Aeronautics and Space Administration Washington, D.C. 20546	14. Sponsoring Agency Code

15. Supplementary Notes

16. Abstract

The results of analog and digital computer studies of a low-pressure-ratio turbojet engine system for use in a drone vehicle are presented. The turbojet engine consists of a four-stage axial compressor, single-stage turbine, and a fixed area exhaust nozzle. Three simplified fuel schedules and a generalized parameter fuel control for the engine system are presented and evaluated. The evaluation is based on the performance of each schedule or control during engine acceleration from a windmill start at Mach 0.8 and 6100 meters (20 000 ft) to 100 percent corrected speed. It was found that, because of the higher acceleration margin permitted by the control, the generalized parameter control exhibited the best dynamic performance.

17. Key Words (Suggested by Author(s))	18. Distribution Statement
Propulsion Controls	Unclassified - unlimited

19. Security Classif. (of this report)	20. Security Classif. (of this page)	21. No. of Pages	22. Price*
Unclassified	Unclassified	55	$3.00

*For sale by the National Technical Information Service, Springfield, Virginia 22151

CONTENTS

PERFORMANCE AND CONTROL STUDY OF A LOW-PRESSURE-RATIO TURBOJET ENGINE FOR A DRONE AIRCRAFT

by Kurt Seldner, Lucille C. Geyser, Harold Gold, Darrel Walker*, and Gary Burgner*

Lewis Research Center

SUMMARY

The results of analog and digital computer studies of a low pressure-ratio turbojet engine system for use in a drone vehicle are presented. The turbojet engine consists of a four-stage axial compressor, single-stage turbine, and a fixed area exhaust nozzle. Three simplified fuel schedules and a generalized parameter fuel control for the engine system are presented and evaluated. The evaluation is based on the performance of each schedule or control during engine acceleration from a windmill start at Mach 0.8 and 6100 meters (20 000 ft) to 100 percent corrected speed. It was found that, because of the higher acceleration margin permitted by the control, the generalized parameter control exhibited the best dynamic performance.

INTRODUCTION

The low-pressure-ratio turbojet engine is a suitable propulsion system for many drone vehicles. The short flight range of most drone missions places minimal requirements on engine fuel consumption. The basic engine simplicity that accompanies the low pressure ratio makes possible low-cost engine construction. Low engine cost is, in turn, a requirement for the economic feasibility of many drone applications.

This report presents the results of a performance and control study of a four to one compression ratio engine operating in a drone vehicle cruising at Mach 0.8 at 6100 meters (20 000 ft) and having a thrust requirement of 1557 newtons (350 lbf). The vehicle was assumed to be started and air launched at the cruise conditions. The design analysis presented was performed on analog and digital computers and is based on the methods described in references 1 and 2.

*Naval Weapons Center, China Lake, California.

This study was made under the Lewis Research Center low-cost engine study program and was performed in cooperation with the Naval Weapons Center, U. S. N.

Design Point Characteristics

In the initial phases of the study, a preliminary cycle analysis based on the computer program of reference 3 was performed on the engine system. This study was used to establish a suitable engine design operating point. Results obtained from this analysis are plotted as variations in specific thrust against specific fuel consumption for several compressor pressure ratios and a range of turbine inlet temperatures in figure 1. A final selection of a pressure ratio of 4 and a turbine inlet temperature of 1078 K (1941° R) was based on the simplicity of the design needed to accommodate system operation at this condition.

Table I presents the actual design data and computed system parameters for various operating conditions. The compressor efficiency and rotational speed are the design values for a four-stage axial-flow transonic compressor. The turbine efficiency is the design value for a single-stage axial-flow machine. The combustor outlet pressure corresponds to an annular combustor with a design pressure loss ratio of 0.055 at the design point.

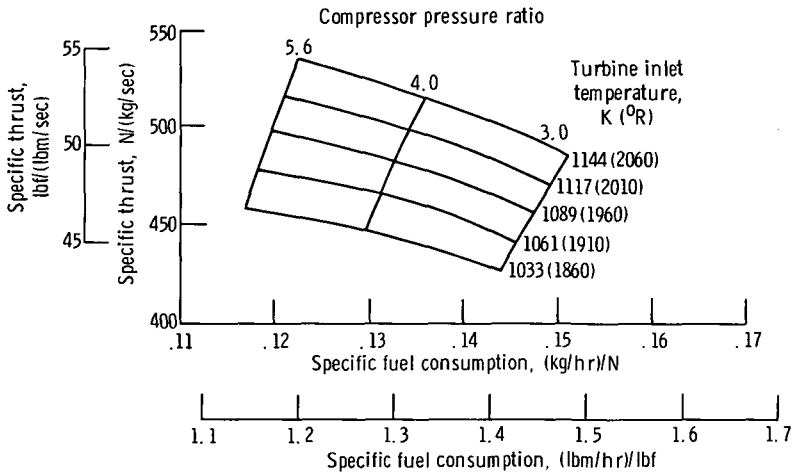

Figure 1. - Specific thrust plotted against specific fuel consumption for drone engine at cruise condition. Mach number, 0.8; altitude, 6100 meters (20 000 ft); pressure ratio difference, 0.99; compressor efficiency, 0.85; combustor efficiency, 0.96; turbine efficiency, 0.88; velocity coefficient, 0.99; combustor $\Delta P/P$, 0.96.

TABLE I. - STEADY-STATE PERFORMANCE

(a) SI units

Condition	1	2	3	4	5
Altitude, m	0	6100	0	0	0
Mach number, M	0	0.8	0.8	0.8	0
Ambient temperature, K	288.3	248.7	288.3	288.3	288.3
Inlet recovery	1.0	0.99	0.99	0.99	1.0
Speed, rpm	35 260	34 800	34 256	35 202	17 630
Percent corrected speed	100	100	91.5	94.0	50.0
Compressor					
Airflow, kg/sec	4.56	3.24	5.83	6.03	1.96
Inlet temperature, K	288.3	280.6	325.1	325.1	288.3
Outlet temperature, K	450.1	437	476.2	485.9	329.3
Inlet pressure, N/m^2	10.13×10^4	7.09×10^4	15.29×10^4	15.29×10^4	10.13×10^4
Pressure ratio	3.96	3.96	3.25	3.45	1.49
Adiabatic efficiency	0.859	0.864	0.861	0.858	0.849
Bleed air, percent	0.0	0.0	0.0	0.0	0.0
Combustor					
Airflow, kg/sec	4.56	3.24	5.83	6.03	1.96
Outlet temperature, K	1118.0	1078.3	1030.6	1098.9	663.3
Outlet pressure, N/m^2	38.09×10^4	26.54×10^4	46.68×10^4	49.62×10^4	14.37×10^4
Fuel flow, kg/hr	300.78	206.47	334.4	374.35	68.08
Turbine					
Gas flow, kg/sec	4.65	3.29	5.93	6.13	1.98
Outlet temperature, K	973.3	945.3	916.7	968.9	627.8
Outlet pressure, N/m^2	20.68×10^4	14.44×10^4	25.61×10^4	27.22×10^4	11.23×10^4
Pressure ratio	1.842	1.84	1.822	1.823	1.279
Adiabatic efficiency	0.85	0.85	0.85	0.85	0.85
Nozzle					
Gas flow, kg/sec	4.65	3.29	5.93	6.13	1.98
Inlet temperature, K	973.3	945.3	916.7	968.9	627.8
Thrust coefficient	0.99	0.99	0.99	0.99	0.99
Performance					
Thrust, N	2864.5	1547.9	2224.0	2664.8	378.1
Specific fuel consumption, (kg/hr)/N	0.107	0.133	0.150	0.141	0.180

TABLE I. - Concluded. STEADY-STATE PERFORMANCE

(b) U. S. Customary units

Condition	1	2	3	4	5
Altitude, ft	0	20 000	0	0	0
Mach number, M	0	0.8	0.8	0.8	0
Ambient temperature, ^{o}R	519.0	447.7	519.0	519.0	519.0
Inlet recovery	1.0	0.99	0.99	0.99	10
Speed, rpm	35 260	34 800	34 256	35 200	17 630
Percent corrected speed	100	100	91.5	94.0	50.0
Compressor					
Airflow, lbm/sec	10.06	7.14	12.86	13.29	4.32
Inlet temperature, ^{o}R	519.0	505.1	585.1	585.1	519.0
Outlet temperature, ^{o}R	810.1	786.6	857.2	874.7	592.8
Inlet pressure, psfa	2116.8	1481.8	3193.9	3193.9	2116.8
Pressure ratio	3.96	3.96	3.25	3.45	1.49
Adiabatic efficiency	0.859	0.864	0.861	0.858	0.849
Bleed air, percent	0.0	0.0	0.0	0.0	0.0
Combustor					
Airflow, lbm/sec	10.06	7.14	12.86	13.29	4.32
Outlet temperature, ^{o}R	2010.0	1941.0	1855.0	1978.0	1194.0
Outlet pressure, psfa	7956.0	5544.0	9748.8	10 363.7	3001.0
Fuel flow, lbm/hr	663.1	455.2	737.2	825.3	150.1
Turbine					
Gas flow, lbm/sec	10.25	7.26	13.06	13.51	4.36
Outlet temperature, ^{o}R	1752.0	1701.5	1650.0	1744.0	1130.0
Outlet pressure, psfa	4318.6	3015.4	5349.6	5685.1	2345.8
Pressure ratio	1.842	1.840	1.822	1.823	1.279
Adiabatic efficiency	0.85	0.85	0.85	0.85	0.85
Nozzle					
Gas flow, lbm/sec	10.25	7.26	13.06	13.51	4.36
Inlet temperature, ^{o}R	1752.0	1701.5	1650.0	1744.0	1130.0
Thrust coefficient	0.99	0.99	0.99	0.99	0.99
Performance					
Thrust, lbf	644.0	348.0	500.0	599.1	85.0
Specific fuel consumption, (lbm/hr)lbf	1.046	1.30	1.47	1.38	1.77

Engine System Simulation

A mathematical description of the turbojet engine system dynamic and steady-state characteristics was formulated and used as the basis for an analog computer simulation. The engine simulation was then used for the investigation of various control schemes over a number of engine operating conditions. Since the system design was to be based on results obtained from the computer model, a comprehensive engine system simulation was developed.

The overall engine system simulation can be regarded as a number of independent, but interconnected, simulations as shown in figure 2. External inputs to the engine sys-

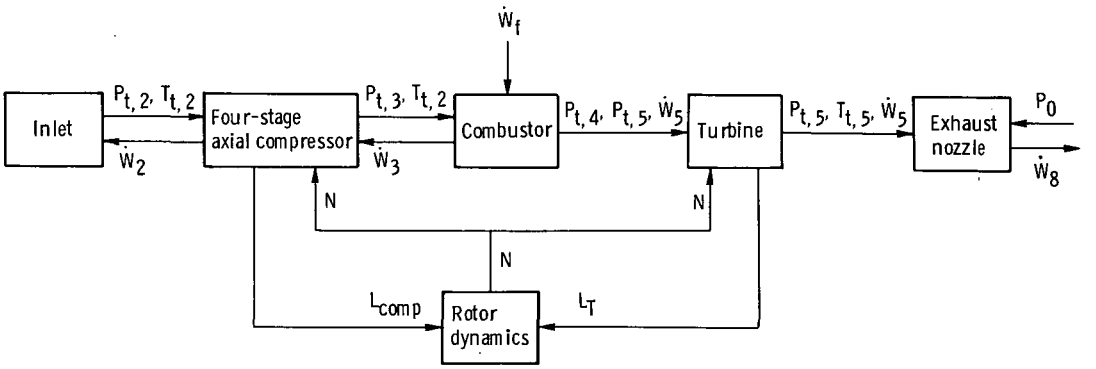

Figure 2. - Simulation diagram for ordnance engine.

tem consist of compressor face conditions and the pressure into which the engine system exhausts. For this study, inlet dynamics were neglected and the compressor face total pressure and temperature were supplied as input constants for each operating condition. The details of the analog computer model are presented in appendix B. In addition to the analog model, a digital program was written in Fortran IV to verify the steady-state portion of the analog results. The digital model also provides a ready means for establishing the effects of engine system modifications on steady-state performance. The digital program is presented in detail in appendix C.

SYSTEM AND CONTROL DISCUSSION

The computer simulation was first applied to determine the engine system steady-state operating characteristics. Once the steady-state performance was established, the model was used to investigate a number of possible fuel control systems.

Steady-State Characteristics

The first simulation runs were used to define the normal engine operating characteristics. Figure 3 presents a compressor map obtained from the simulation. The compressor map was generated by holding rotor speed constant and varying the compressor exit impedance. The resulting variation in pressure ratio was plotted against corrected weight flow, and a constant speed operating line was thus obtained. The process was repeated for a series of rotor speeds to form the complete map. As indicated in references 1 and 2, the compressor simulation technique applied in this system simulation can be used to define the compressor stall line. The stability boundary of the compressor simulation will closely match the compressor stall line. This stability boundary is included in figure 3.

The engine normal operating line for 6100 meters (20 000 ft) and M = 0.8 was also included in figure 3. This line is the locus of steady-state operating points plotted in the coordinates of the compressor map. The operating line shown in figure 3 illustrates engine performance at design conditions. As inlet conditions and exhaust nozzle area vary, the normal operating line will shift.

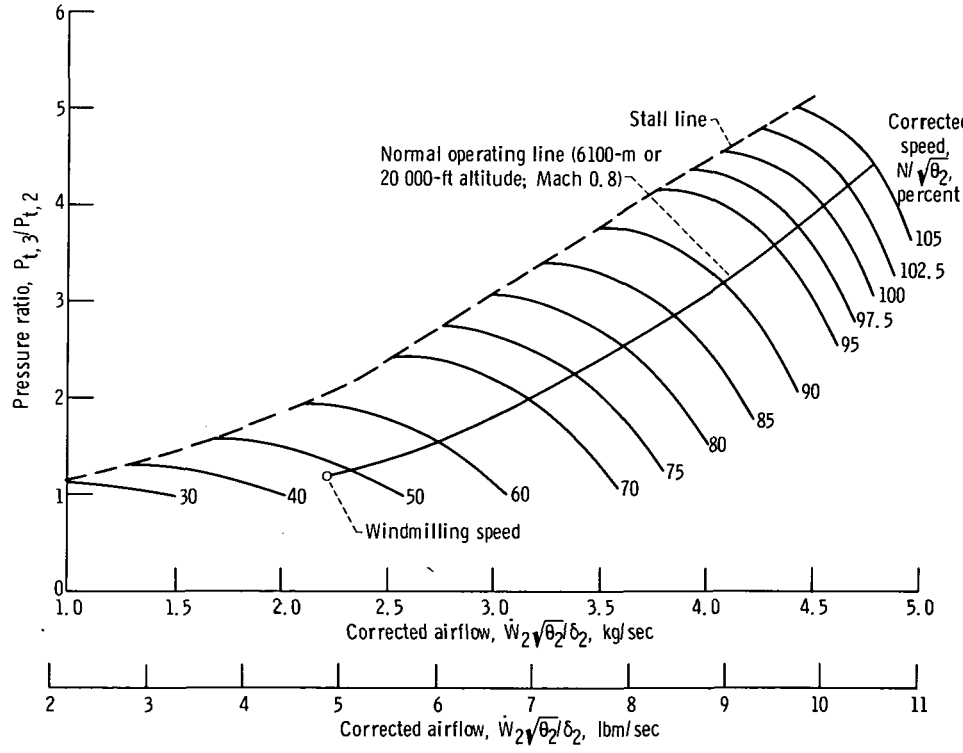

Figure 3. - Compressor map for drone engine.

Engine normal operating lines were determined for a number of operating conditions, and are plotted on a steady-state compressor map in figure 4. The operating line for sea-level static conditions intersects the compressor stall line at 41. 5 percent corrected speed. The effect of inlet ram pressure, however, is to shift the operating line away from the surge line, such that there is sufficient surge margin at all Mach numbers greater than 0. 5 and corrected speeds greater than the windmilling speed. It must be recognized that the component data used in the computer model is preliminary. Final data for the engine model could shift the surge and normal operating lines.

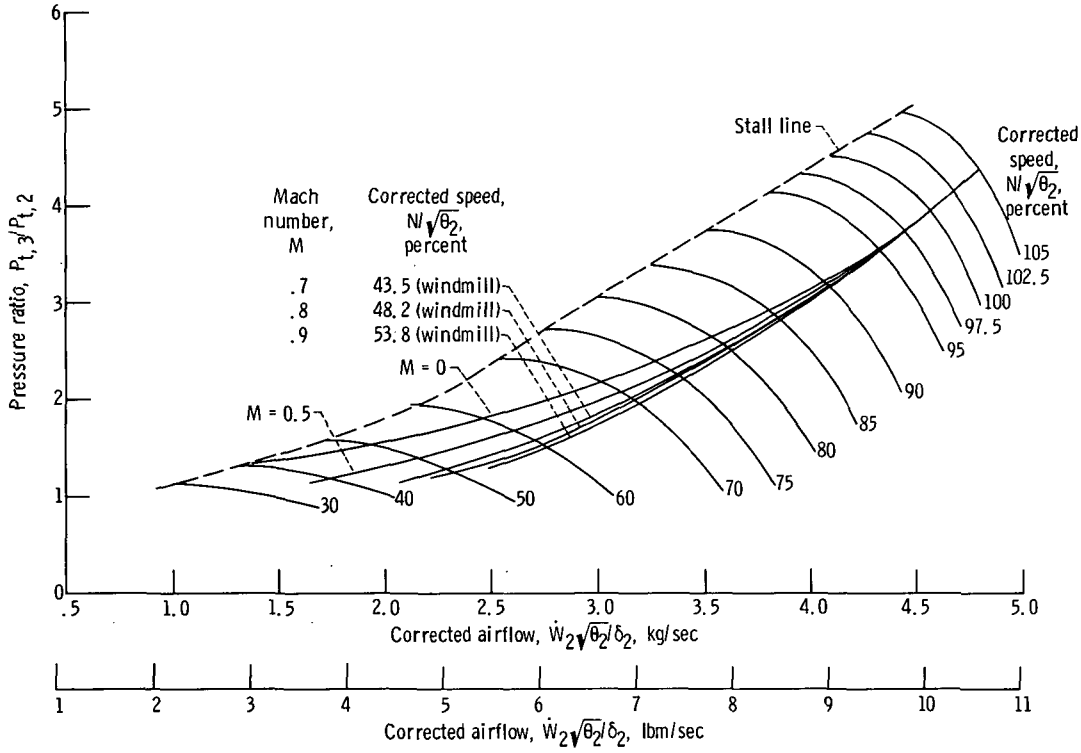

Figure 4. - Compressor map with normal operating lines for sea-level and altitude conditions.

The effect of varying the exhaust nozzle area at sea-level static conditions was investigated. These results, shown in figure 5(a) indicate that additional surge margin, particularly at high rotor speeds, can be gained. However, the design point compressor performance varies with exhaust nozzle area. Figure 5(b) presents lines of constant turbine inlet temperature superimposed on the compressor map. These data were obtained by varying fuel flow and exhaust nozzle area to establish an engine operating speed and a turbine inlet temperature. The normal operating line for the cruise condition is included for reference.

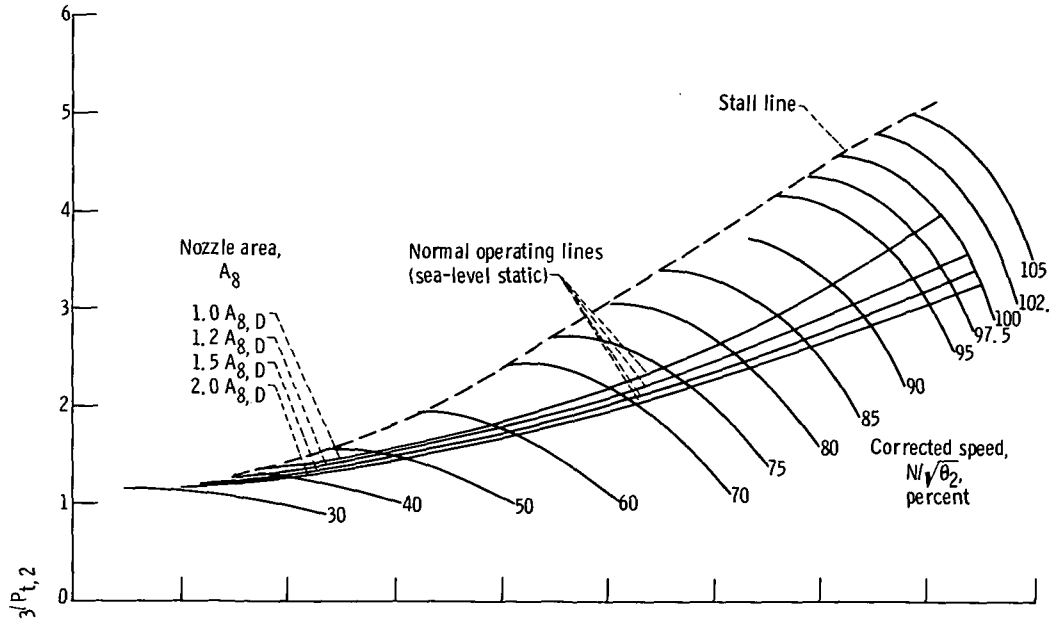

(a) Variation of normal operating line with exhaust nozzle area.

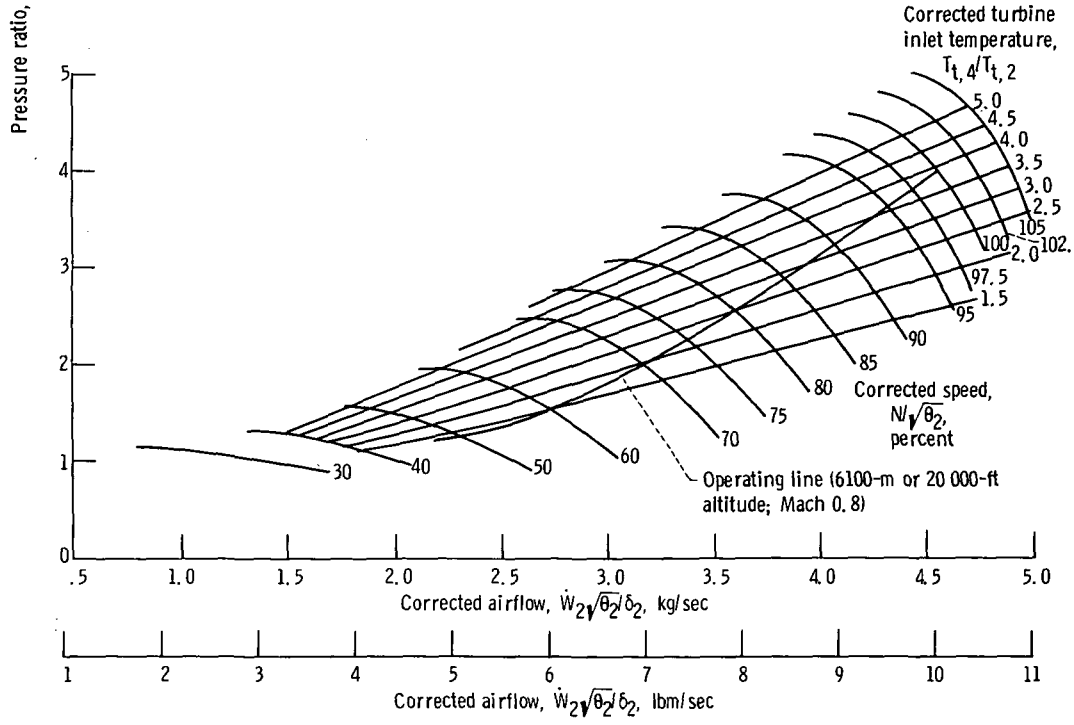

(b) Constant turbine inlet temperature lines.

Figure 5. - Compressor map for drone engine.

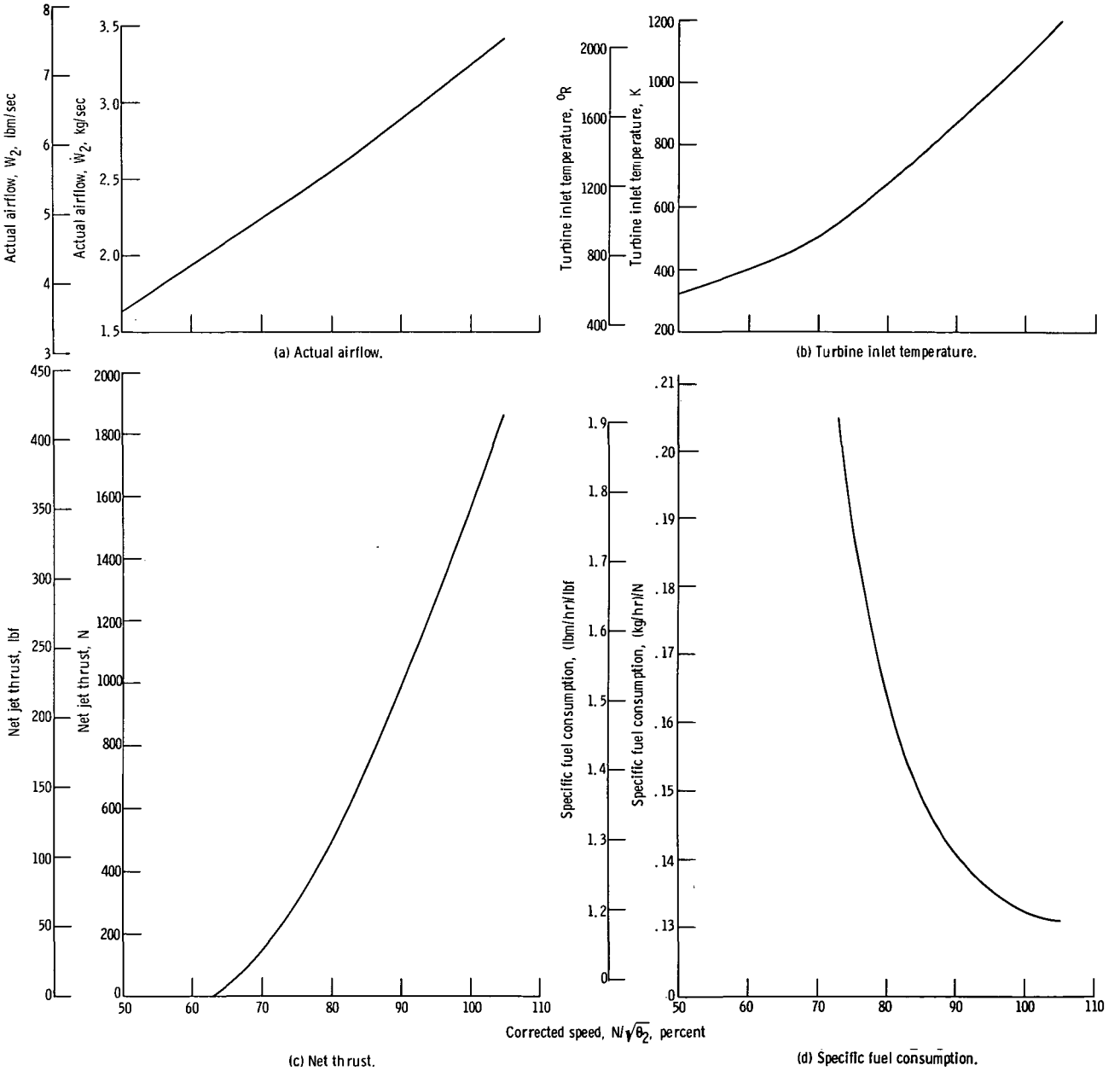

(a) Actual airflow.

(b) Turbine inlet temperature.

(c) Net thrust.

(d) Specific fuel consumption.

Figure 6. - Drone engine performance at cruise condition.

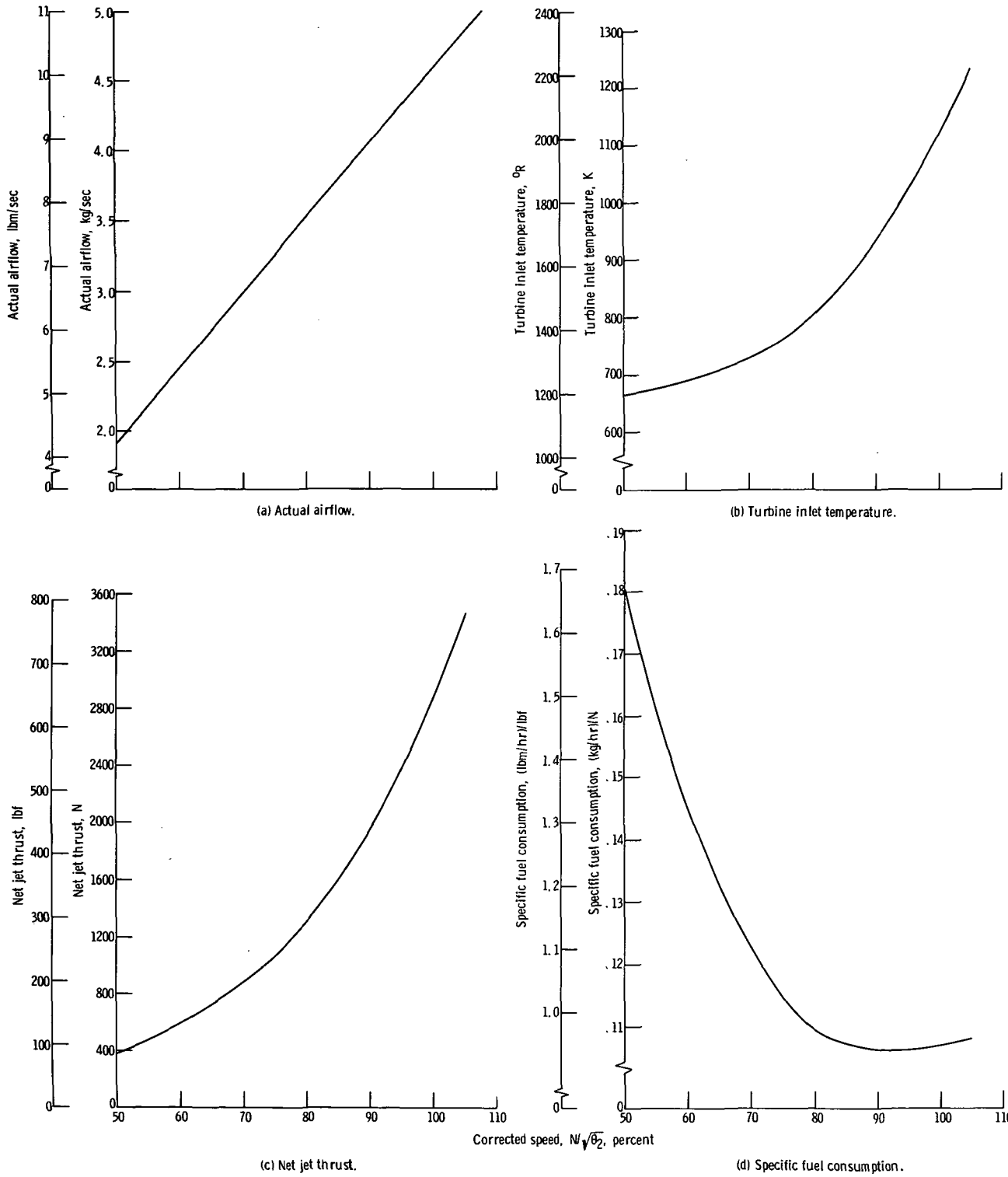

(a) Actual airflow.

(b) Turbine inlet temperature.

(c) Net jet thrust.

(d) Specific fuel consumption.

Figure 7. - Drone engine performance at sea-level static condition.

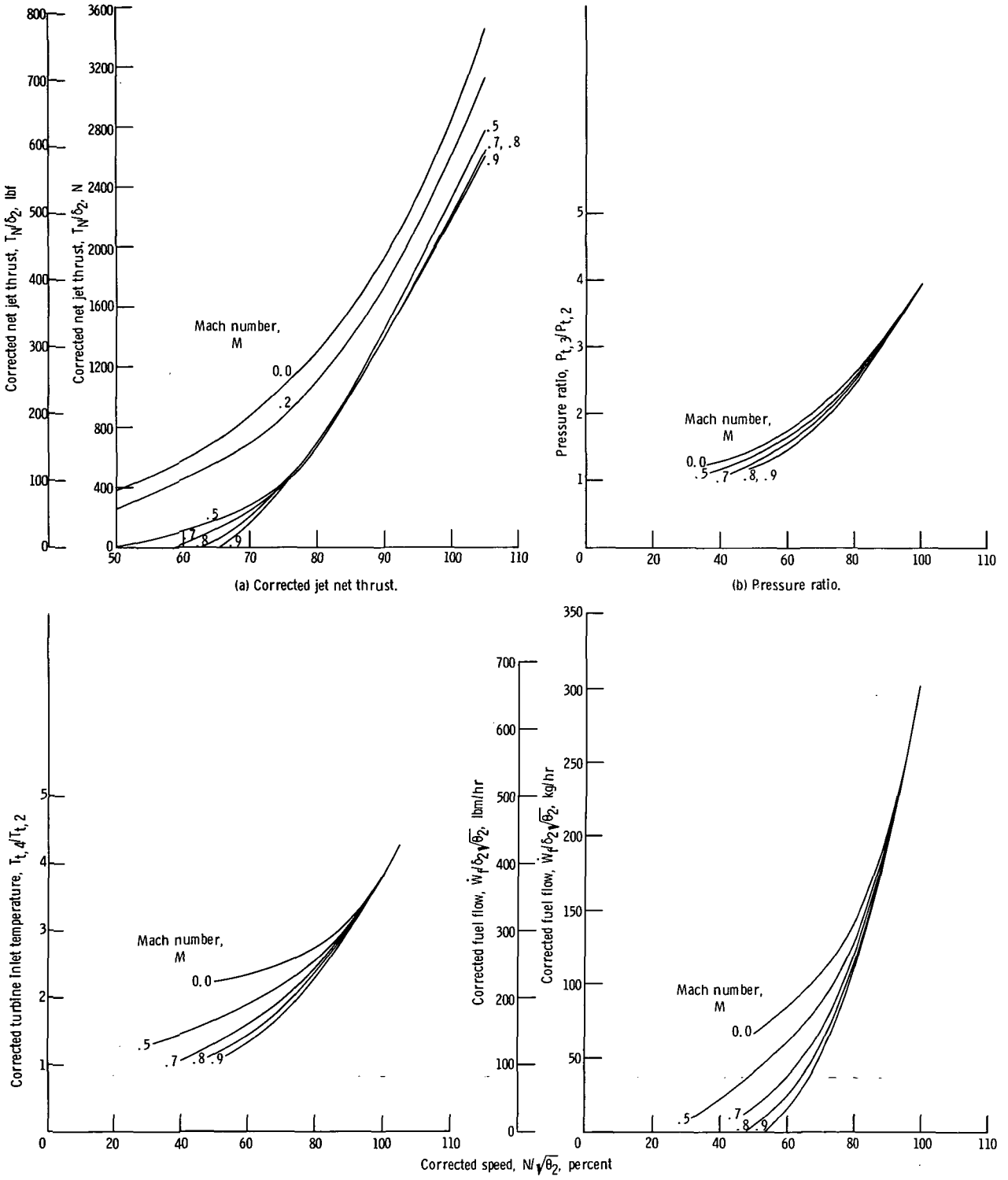

Figure 8. - Corrected performance parameters for various flight conditions.

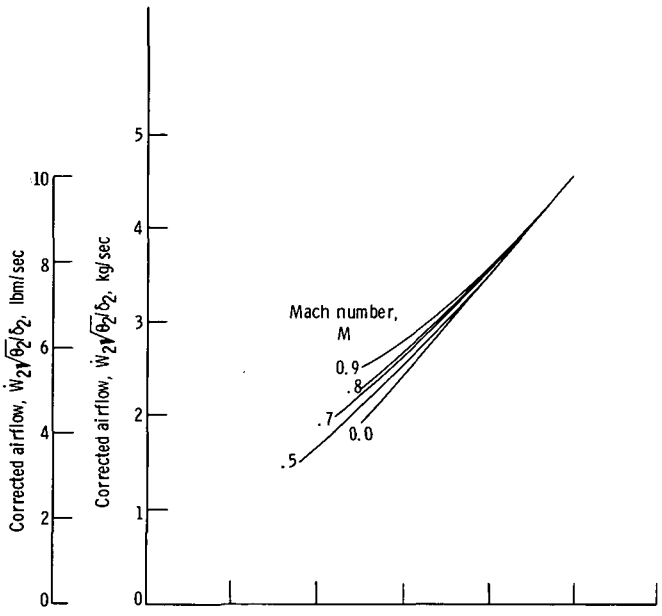

(e) Corrected airflow.

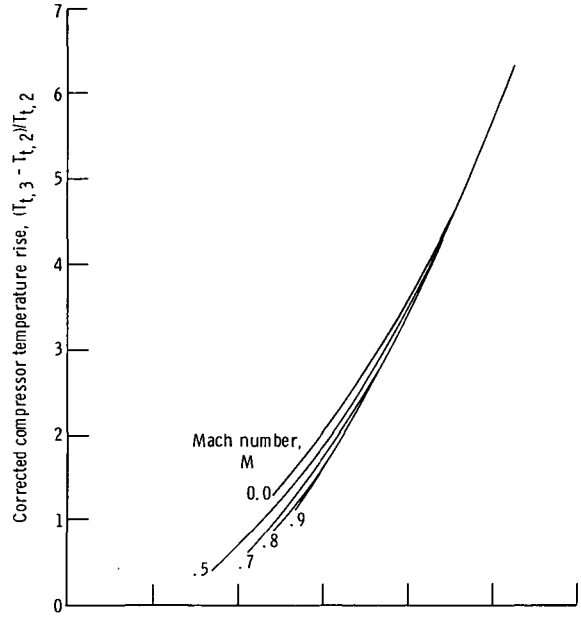

(f) Compressor temperature rise.

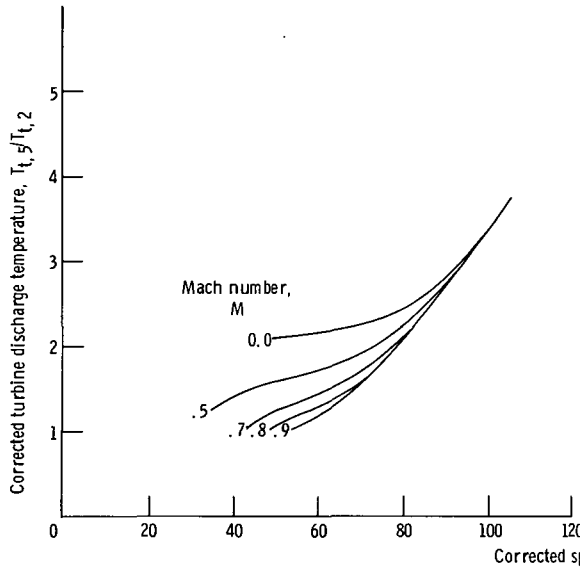

(g) Corrected turbine discharge temperature.

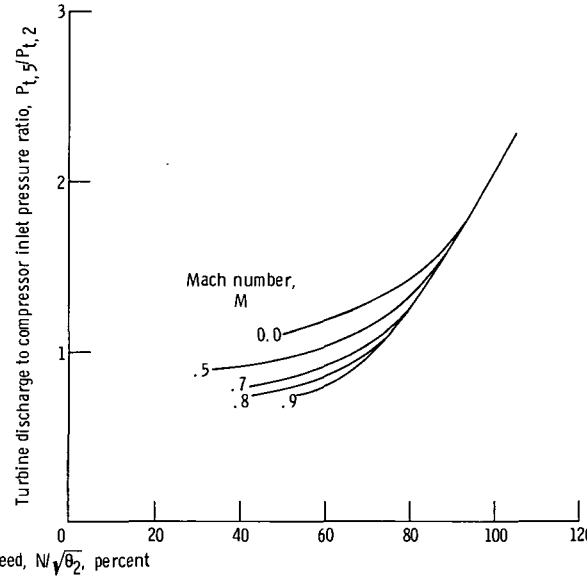

(h) Turbine discharge to compressor inlet pressure ratio.

Figure 8. - Concluded.

The predicted propulsion system performance at Mach 0.8 and 6100 meters (20 000 ft) is shown in figure 6. At 100 percent corrected speed, a turbine inlet temperature of 1078 K (1941° R), pressure ratio of 3.96, and airflow of 3.24 kilogram per second (7.14 lbm/sec), the thrust (with a converging nozzle) is equal to 1548 newtons (348 lbf) with a specific fuel consumption of 0.133 kilogram per hour per newton (1.30 (lbm/hr)/lbf). All performance predictions are for a nozzle exit area of 0.0182 square meter (0.1963 ft^2) and an inlet total pressure recovery of 1.0.

The system performance at sea-level static conditions is shown in figure 7. At 100 percent corrected speed, a pressure ratio of 3.96, and a turbine inlet temperature of 1117 K (2010° R), the thrust is 2865 newtons (644 lbf) with a specific fuel consumption of 0.107 kilogram per hour per newton (1.046 (lbm/hr)/lbf).

Figure 8 presents the significant engine corrected performance parameters as a function of corrected speed for several flight conditions. These characteristics were obtained for an inlet total pressure recovery of 1.0 and an exhaust nozzle area of 0.0182 square meter (0.1963 ft^2).

Windmilling Characteristics

The simulation of the turbojet engine provided a convenient means of studying the free windmilling condition under various flight conditions. Of particular interest are the rotor speed, air flow, and combustor pressure and temperature. The windmill condition is achieved by simply reducing the fuel flow to zero and permitting the compressor and turbine torque to come to an equilibrium balance.

It should be noted, however, that windmill conditions are difficult to estimate accurately. At windmill, both the compressor and turbine performance must be estimated far from the design point; in addition, the computer voltage levels are low, all of which introduce computational inaccuracies.

For an engine which is to be started or restarted in flight from the windmilling condition, it is important to know the surge margin, air flow, and combustor pressure and temperature from the standpoint of combustor and igniter design and fuel scheduling. The combustion and igniter must be designed to ensure satisfactory ignition at the most severe windmilling condition anticipated, and the fuel-air mixture must be limited to values which preclude compressor stalling upon ignition. Further, the structural integrity of the rotor, particularly bearings, may be influenced by the windmilling condition.

It was discovered that for all conditions investigated, the corrected windmill rotor speed is proportional to flight speed (fig. 9(a)). Corrected air flow through the engine, however, is a function only of flight Mach number (fig. 9(b)). Combustor pressure and compressor discharge temperature at the windmill condition are presented in figures 9(c) and (d), respectively, for the anticipated range of flight conditions.

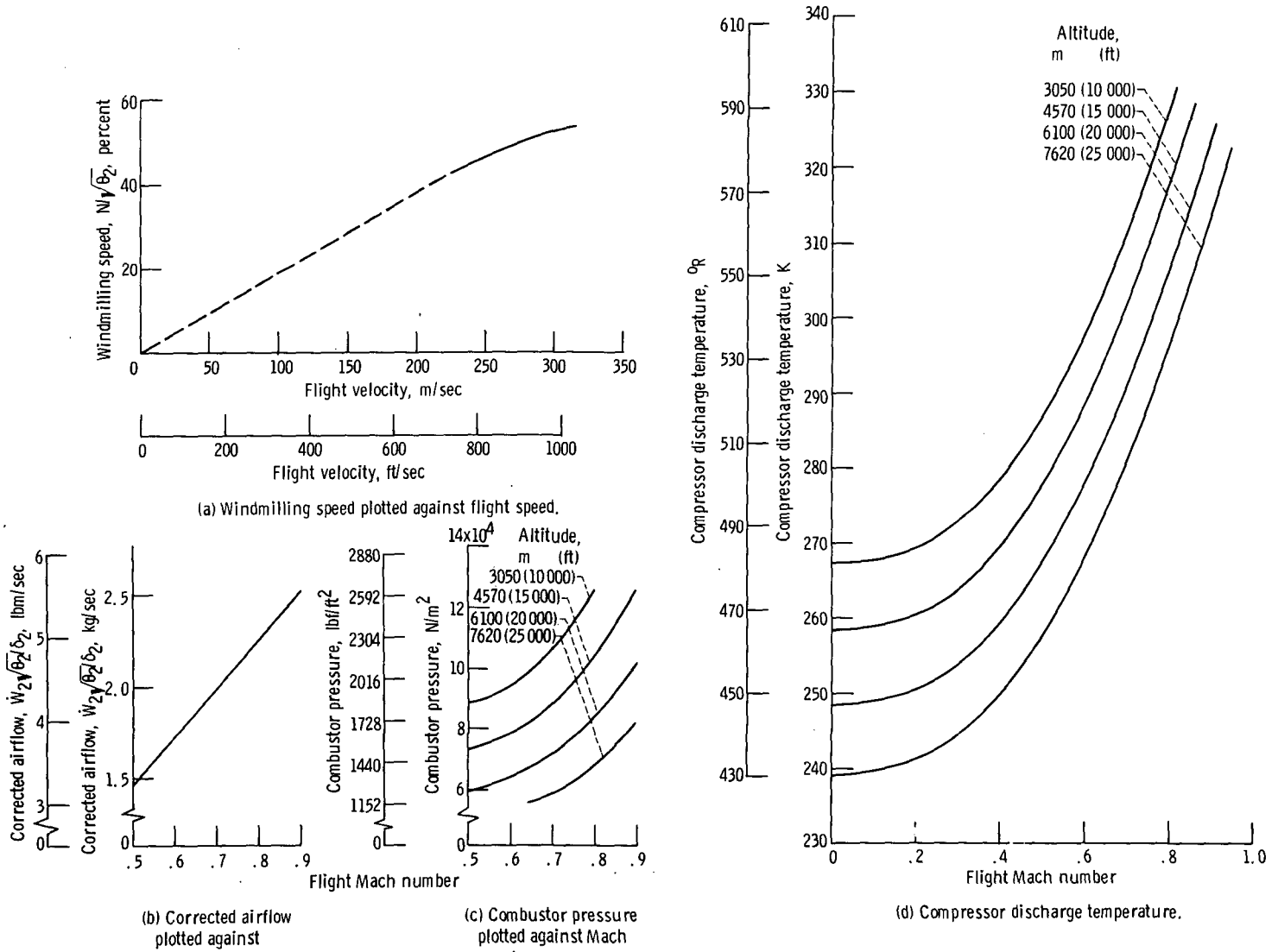

(a) Windmilling speed plotted against flight speed.

(b) Corrected airflow plotted against Mach number.

(c) Combustor pressure plotted against Mach number.

(d) Compressor discharge temperature.

Figure 9. - Windmill data for drone engine.

Fuel Controls

In addition to the investigation of basic engine performance characteristics, the simulation was used to evaluate various engine fuel schedules and controls. Engine control concepts were examined for a specific application in which the engine would be started from the windmill condition in flight and, once started, would operate continuously at or near full thrust.

The application requires a fuel schedule which supplies a prescribed amount of fuel as a function of the engine operating state. The fuel supplied must maintain engine operation within safe operating limits during acceleration. The application does not necessarily require closed loop control and, if possible, should be satisfied by a simple fuel schedule. Several fuel controls were investigated with the system simulation. Three of these controls consisted of open loop fuel flow schedules, based on different engine parameters. The fourth control was a generalized parameter fuel control, which was a more conventional closed loop system.

The basic criteria used to evaluate the concepts was the ability to provide adequate acceleration within the compressor stall limit and to maintain the engine near design speed for cruise conditions between $M = 0.9$ at 4570 meters (15 000 ft) and $M = 0.7$ at 7620 meters (25 000 ft).

The selected fuel schedules are based on linear relations of a fuel flow parameter and compressor pressure ratio. These relations were arbitrarily selected using previous control experience.

Case A fuel control. - The case A fuel schedule was based on the corrected parameter plots of figure 10. The curves plotted in this figure represent the system normal operating lines for various flight Mach numbers. These lines are represented in terms of a fuel flow parameter $\dot{W}_f/N\delta_2$ and the compressor pressure ratio $P_{t,3}/P_{t,2}$. A point on a curve represents an equilibrium operating condition at a given flight Mach number, while a point above a normal operating line represents more fuel than required for equilibrium and, hence, system acceleration capability.

The various normal operating lines converge to a single line as operation approaches the design compressor pressure ratio of 3.96. It is evident from figure 10 that a linear schedule of the fuel flow parameter (dashed line) intersecting the normal operating line at the design point can be used to control the engine. This type of linear fuel schedule requires only the measurement of compressor inlet and discharge pressures and engine speed. The acceleration schedule must be above the normal operating lines to provide excess fuel to accelerate the system. The slope of the acceleration schedule was selected such that the engine is capable of accelerating from about 50 percent speed at sea-level conditions.

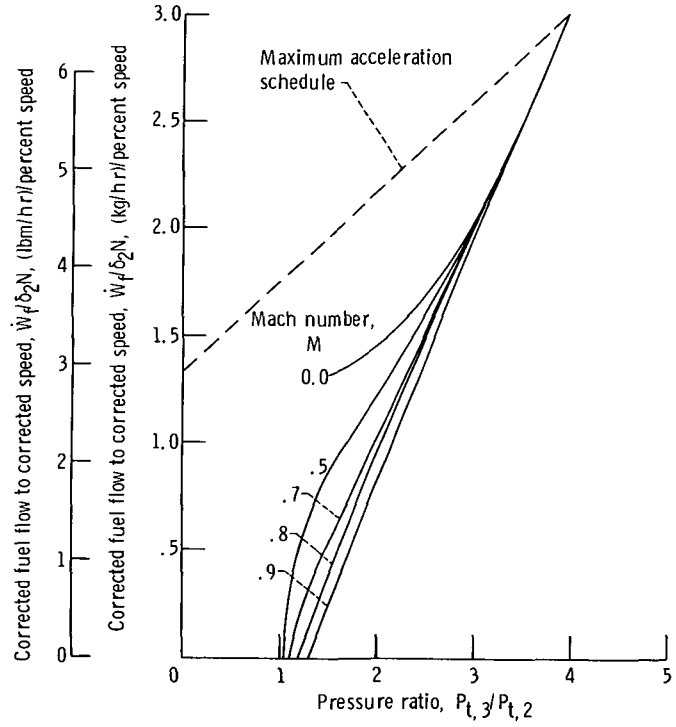

Figure 10. - Engine corrected fuel flow to corrected speed requirements for various flight Mach numbers.

Using these constraints, the fuel schedule was based on the relation

$$\left.\begin{aligned} \frac{\dot{W}_f}{N\delta_2} &= 1.33 + 0.420\,\frac{P_{t,3}}{P_{t,2}} \qquad \text{(kg/hr)/percent speed} \\ \frac{\dot{W}_f}{N\delta_2} &= 2.93 + 0.925\,\frac{P_{t,3}}{P_{t,2}} \qquad \text{(lbm/hr)/percent speed} \end{aligned}\right\} \quad (1)$$

These equations can be written as

$$\left.\begin{aligned} \dot{W}_f &= N\left(0.1311\times10^{-4}\,P_{t,2} + 0.0414\times10^{-4}\,P_{t,3}\right) \qquad \text{kg/hr} \\ \dot{W}_f &= N\left(1.384\times10^{-3}\,P_{t,2} + 0.437\times10^{-3}\,P_{t,3}\right) \qquad \text{lbm/hr} \end{aligned}\right\} \quad (2)$$

The aforementioned fuel schedule will accelerate the engine from windmilling to design speed and provide the correct fuel flow to maintain the engine at 100 percent corrected speed for all flight conditions.

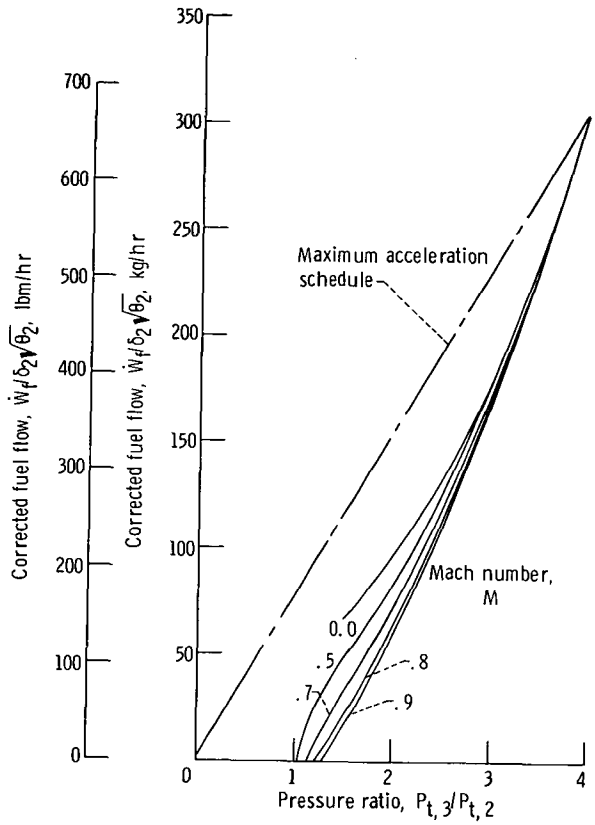

Figure 11. - Engine corrected fuel flow requirements for various flight Mach numbers.

Case B-fuel control. - The effects of scheduling the corrected fuel flow parameter $\dot{W}_f/\delta_2\sqrt{\theta_2}$ as a function of compressor pressure ratio was also investigated. Figure 11 presents normal operating lines for various flight Mach numbers plotted in terms of these parameters. It can be seen in figure 11 that the normal operating lines also converge to a single line as the design pressure ratio is approached. As with the case A fuel control, a linear fuel schedule through the design point and above the family of operating lines can be used.

The case B fuel control was then based on a linear schedule of $\dot{W}_f/\delta_2\sqrt{\theta_2}$ against $P_{t,3}/P_{t,2}$. The schedule for the case B control was adjusted to provide the correct fuel flow at 100 percent corrected speed. The equation for this control schedule is

$$\left.\begin{aligned} \frac{\dot{W}_f}{\delta_2\sqrt{\theta_2}} &= 2.4 + 74.91\frac{P_{t,3}}{P_{t,2}} \qquad \text{kg/hr} \\ \frac{\dot{W}_f}{\delta_2\sqrt{\theta_2}} &= 5.29 + 165.14\frac{P_{t,3}}{P_{t,2}} \qquad \text{lbm/hr} \end{aligned}\right\} \tag{3}$$

or

$$\left.\begin{aligned} \dot{W}_f &= \sqrt{\theta_2}\left(0.2369\times10^{-4}\, P_{t,2} + 7.391\times10^{-4}\, P_{t,3}\right) && \text{kg/hr} \\ \dot{W}_f &= \sqrt{\theta_2}\left(2.50\times10^{-3}\, P_{t,2} + 78.01\times10^{-3}\, P_{t,3}\right) && \text{lbm/hr} \end{aligned}\right\} \quad (4)$$

A direct mechanization of the fuel schedules given by equations (3) and (4) requires measurement of the compressor inlet total temperature. For the computer analysis, however, the $\sqrt{\theta_2}$ term was neglected. The schedule thus reduces to:

$$\left.\begin{aligned} \dot{W}_f &= \left(0.2369\times10^{-4}\, P_{t,2} + 7.391\times10^{-4}\, P_{t,3}\right) && \text{kg/hr} \\ \dot{W}_f &= \left(2.50\times10^{-3}\, P_{t,2} + 78.01\times10^{-3}\, P_{t,3}\right) && \text{lbm/hr} \end{aligned}\right\} \quad (5)$$

The effects of neglecting the variation in compressor inlet temperature were examined during the computer study. The acceleration characteristics obtained with this fuel schedule are acceptable. The correct amount of fuel is supplied to maintain the engine within ±2.5 percent of design speed of all flight conditions. The fuel schedule requires measurement of the compressor inlet and discharge pressure conditions.

Case C fuel control. - A minor variation of the case B fuel schedule was also investigated. From figure 11, it can be noted that the fuel flow intercept is extremely low and thus could be neglected. A linear fuel schedule of the following equation form was considered:

$$\frac{\dot{W}_f}{\delta_2\sqrt{\theta_2}} = b\,\frac{P_{t,3}}{P_{t,2}} \quad (6)$$

or, again neglecting the temperature effects,

$$\left.\begin{aligned} \dot{W}_f &= 0.7350\times10^{-3}\, P_{t,3} && \text{kg/hr} \\ \dot{W}_f &= 77.57\times10^{-3}\, P_{t,3} && \text{lbm/hr} \end{aligned}\right\} \quad (7)$$

Generalized parameter control. - The controls discussed thus far schedule fuel flow as a function of engine parameters. The schedules presented result in engine acceleration and operation close to the design speed. Operation at other engine speeds, however, is not possible. The generalized parameter fuel control of reference 4 allows a more

complete engine control. This control was adapted for use with the drone engine, and simulated on the analog computer with the drone simulation. The generalized parameter fuel control consists of a series-parallel combination of orifices used to generate the desired control limits. The concept is based on the assumption that the maximum and minimum fuel limits can be described as linear functions of corrected engine parameters.

The acceleration limit is defined by the following relation:

$$\left.\begin{aligned} \frac{\dot{W}_f}{\delta_2\sqrt{\theta_2}} &= \frac{N}{\sqrt{\theta_2}}\left(0.7439\,\frac{P_{t,3}}{P_{t,2}} + 0.6804\right) && \text{(kg/hr)/percent speed} \\ \frac{\dot{W}_f}{\delta_2\sqrt{\theta_2}} &= \frac{N}{\sqrt{\theta_2}}\left(1.64\,\frac{P_{t,3}}{P_{t,2}} + 1.50\right) && \text{(lbm/hr)/percent speed} \end{aligned}\right\} \quad (10)$$

and the minimum fuel limit is defined by

$$\left.\begin{aligned} \frac{\dot{W}_f}{\delta_2\sqrt{\theta_2}} &= \frac{N}{\sqrt{\theta_2}}\left(0.404\,\frac{P_{t,3}}{P_{t,2}} - 0.404 + \frac{2.94\times10^4}{P_{t,2}}\right) && \text{(kg/hr)/percent speed} \\ \frac{\dot{W}_f}{\delta_2\sqrt{\theta_2}} &= \frac{N}{\sqrt{\theta_2}}\left(0.89\,\frac{P_{t,3}}{P_{t,2}} - 0.89 + \frac{1355}{P_{t,2}}\right) && \text{(lbm/hr)/percent speed} \end{aligned}\right\} \quad (11)$$

Dynamic Response of Engine and Fuel Controls

A computer investigation of critical engine parameters during acceleration from windmill to full speed with the various fuel controls was made. The objective of this study was to establish the dynamic response of the engine system during the acceleration transient and to compare the different controls.

The acceleration characteristics obtained from the engine and the generalized parameter fuel control are presented first. As indicated in reference 4, this control concept results in engine dynamic performance similar to that obtained with conventional fuel controls. The data with this control is thus presented first to provide a basis for the evaluation of the other simplified fuel controls investigated.

The operating characteristic obtained with the drone engine and the generalized parameter control, during acceleration from windmill to design speed at the cruise condition is presented in figure 12(a). For the large throttle advances represented by this transient, the governor spool travel is limited and acceleration occurs along the maxi-

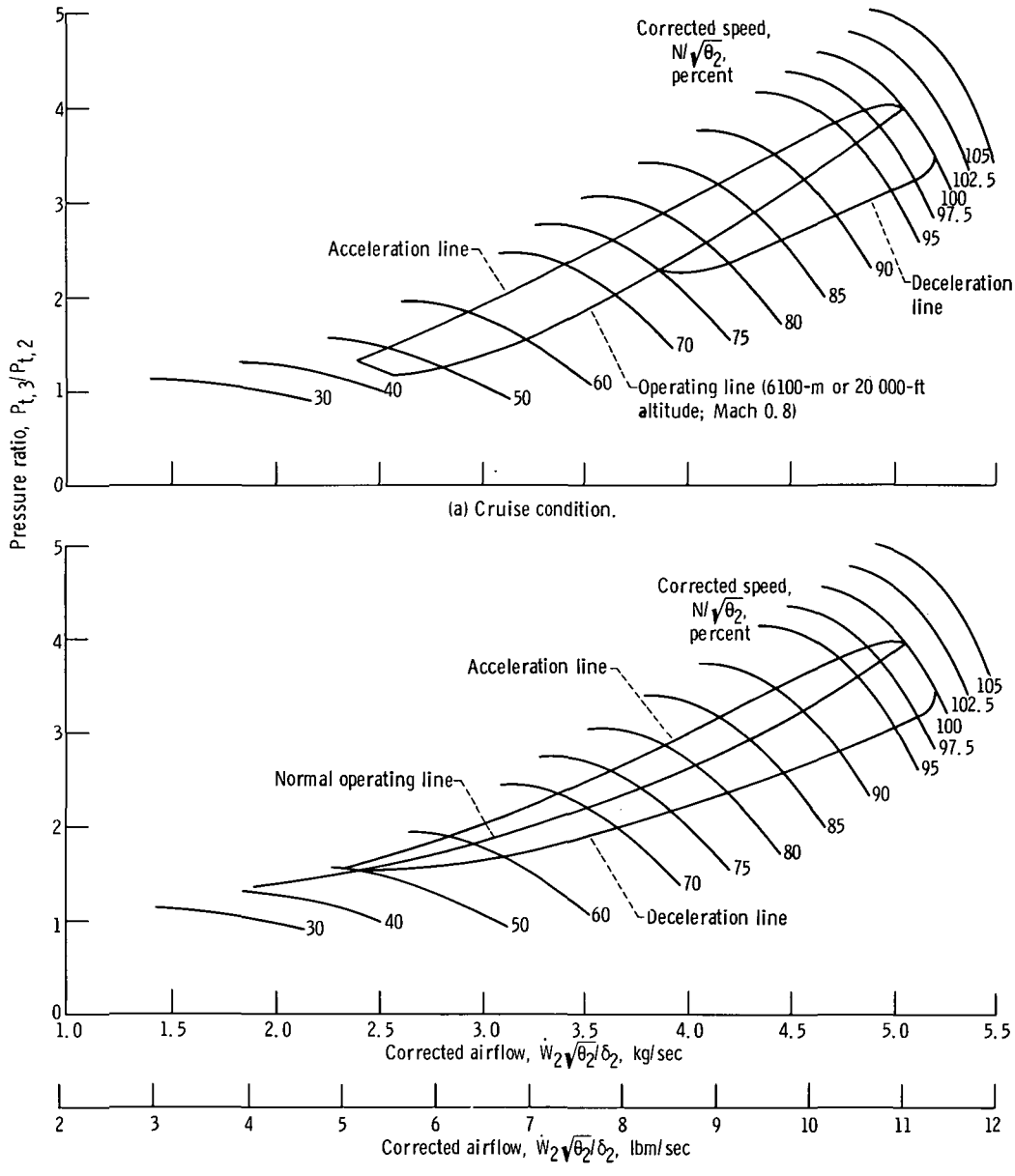

(a) Cruise condition.

(b) Sea-level condition.

Figure 12. - Acceleration and deceleration characteristics with generalized parameter control.

mum fuel limit to the desired speed. The engine deceleration characteristic from design to 75 percent speed is also shown in figure 12(a).

Similar acceleration and deceleration characteristics at sea-level static are presented in figure 12(b). The acceleration characteristics for cruise and sea-level static are shown on a fuel parameter to pressure ratio plot in figure 13. The linear relations for the maximum and minimum fuel limits are evident in this figure.

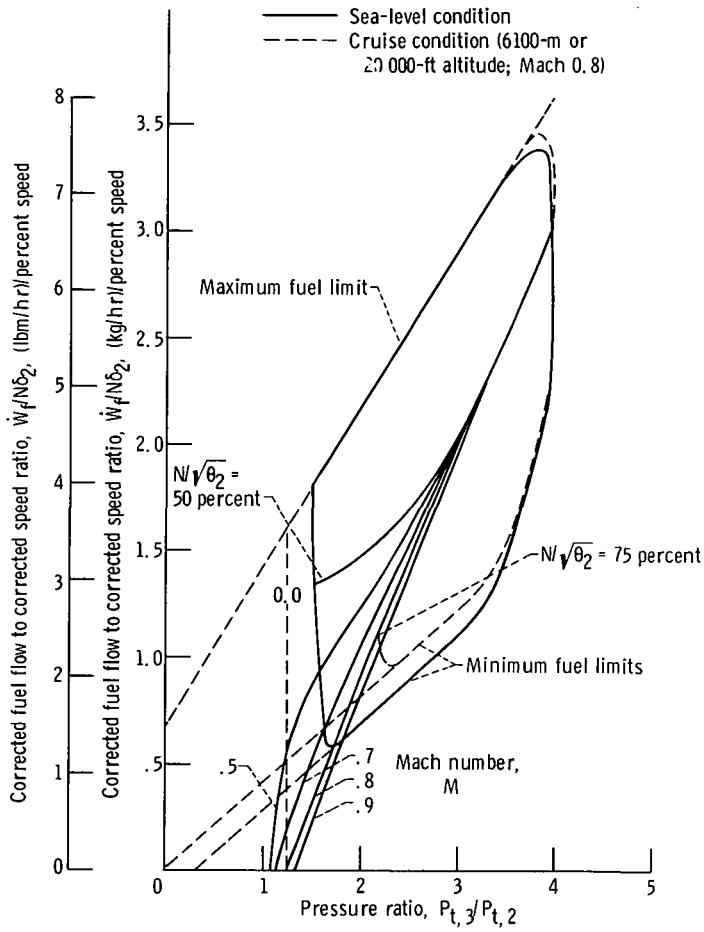

Figure 13. - Acceleration characteristics of drone engine with generalized parameter control.

In general, the acceleration characteristics exhibited by each of the three pressure-related fuel controls (A, B, and C) were found to be similar. Figure 14(a) shows the acceleration lines for each of the three, and for the generalized parameter fuel control, plotted on a compressor map. The engine normal operating line and the compressor stall line are also included in the plot, thus giving a relative indication of the available acceleration and stall margins. The characteristics are plotted for the cruise condition

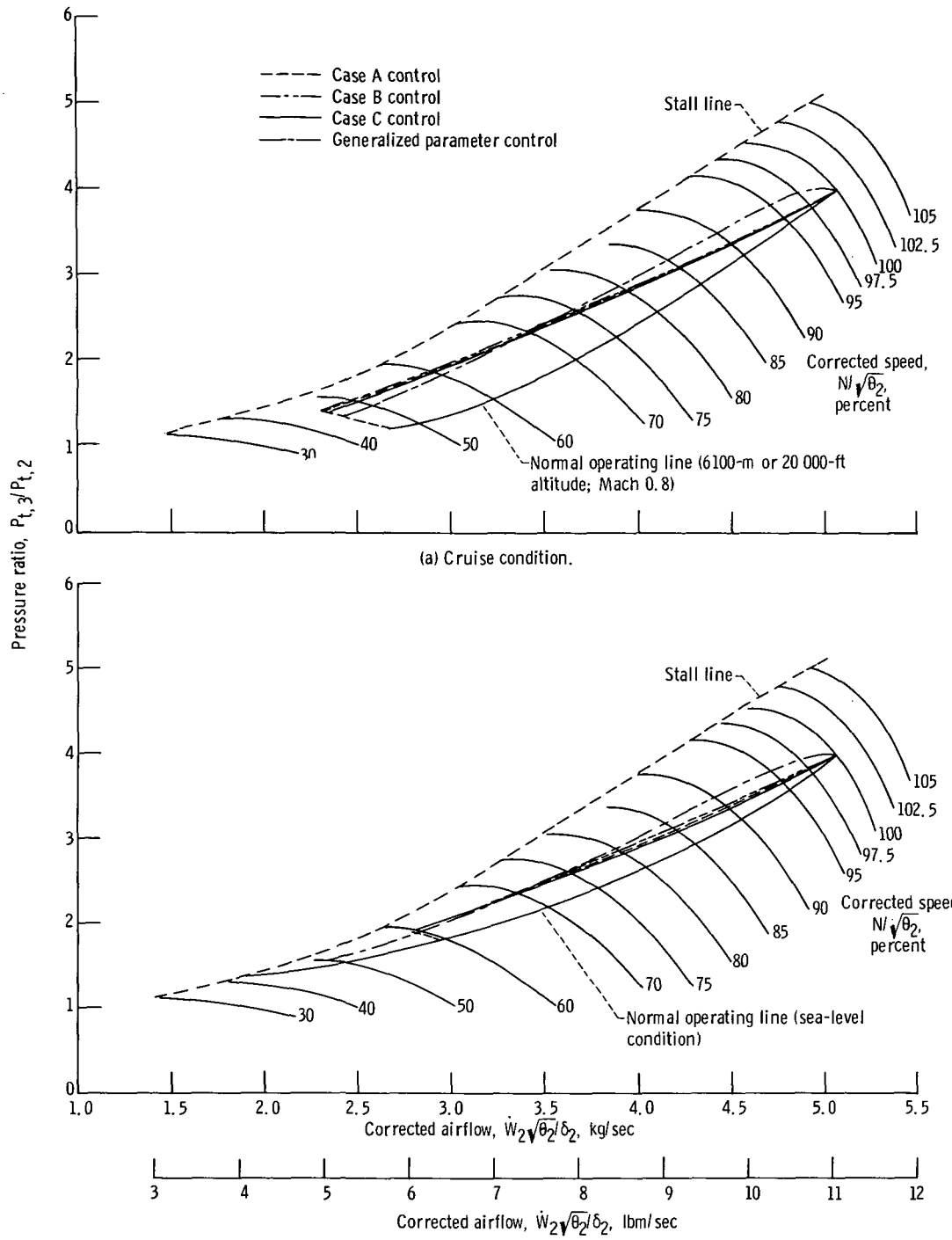

Figure 14. - Acceleration characteristics for various control schedules.

of M = 0.8 at 6100 meters (20 000 ft). The fuel schedules for the three simplified controls are nearly equivalent and the time to accelerate the engine from windmill to full speed was approximately 4 seconds for each of the three. The acceleration line for the generalized parameter fuel control crosses the lines generated by the simplified controls at about 70 percent corrected speed. The more conventional control (generalized parameter) thus provides higher fuel flow above 70 percent speed and yields a somewhat faster acceleration transient.

The acceleration characteristics for the four controls are presented for sea-level static conditions in figure 14(b). At this operating condition the engine normal operating line and the acceleration lines are closer to the compressor stall line in the low speed range than they were at the cruise condition. Because of the resulting low surge margin at the windmill condition, engine accelerations were made from an idle condition at 60 percent corrected speed. The general trends, however, were found to be similar to those obtained at the cruise condition.

The transient acceleration performance of the drone engine was investigated at the cruise altitude condition. As an example, the fuel schedule B was selected to illustrate the transient performance from windmilling to design speed. Typical responses of significant engine variables are presented in figure 15. Immediately after ignition, the

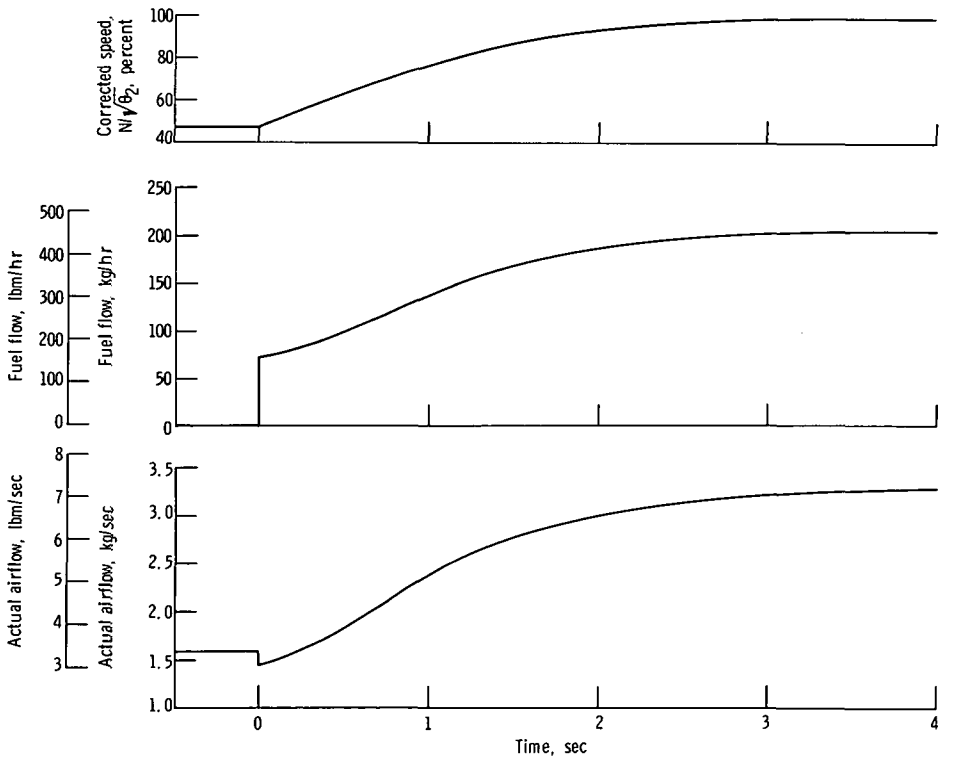

(a) Speed, fuel flow, and actual airflow transients.

Figure 15. - Acceleration characteristics with fuel schedule B at 6100-meter (20 000-ft) altitude and Mach 0.8 from windmilling to design speed.

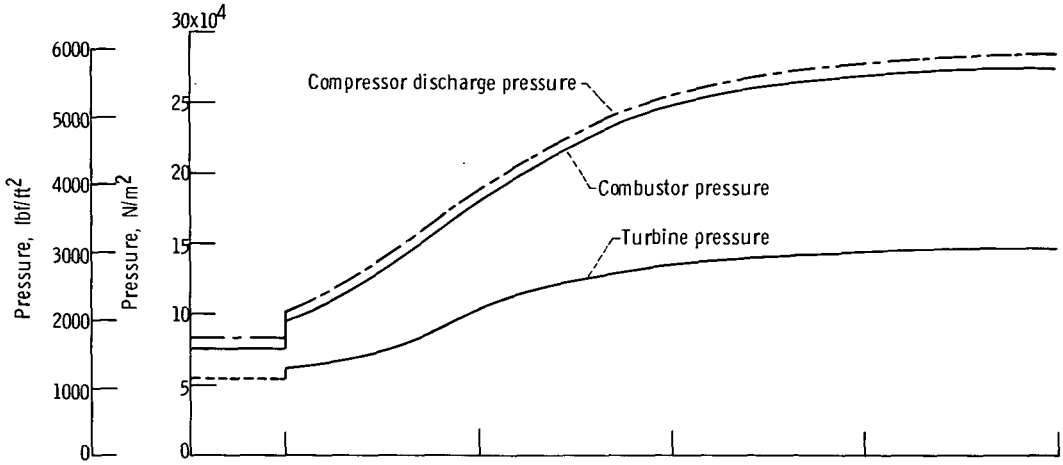

(b) Pressure transients.

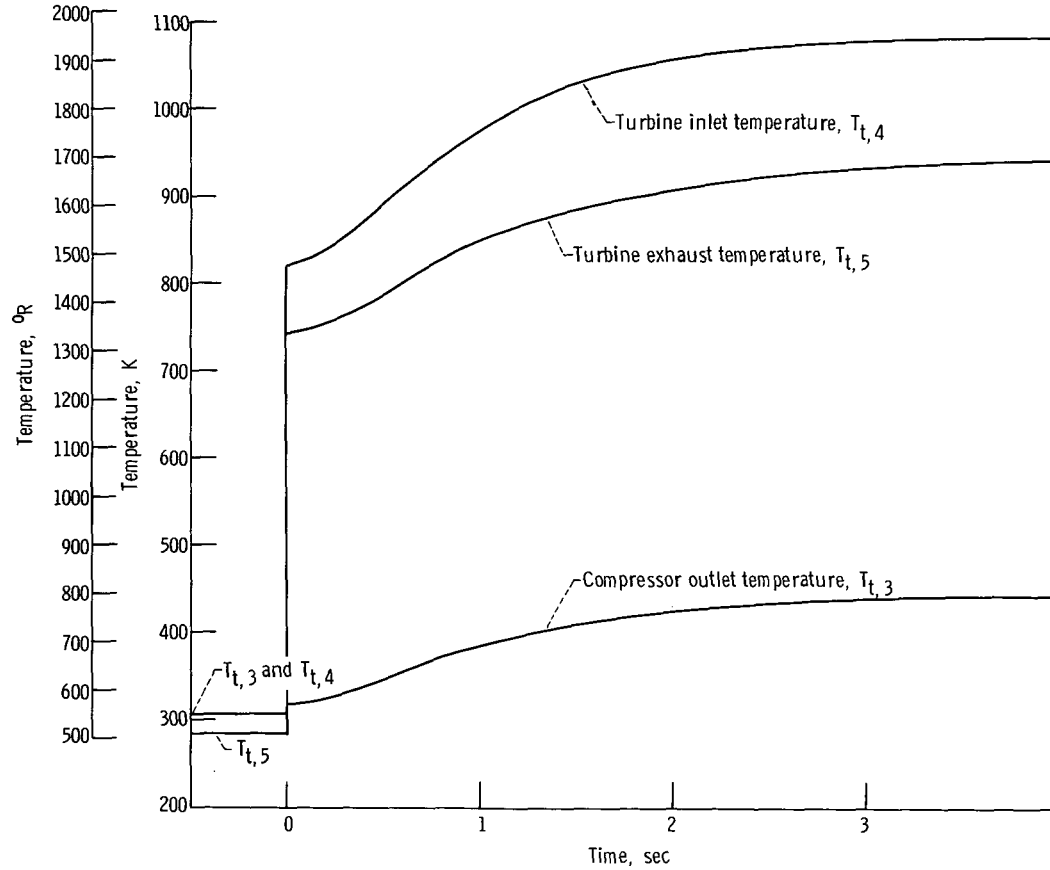

(c) Temperature transients.

Figure 15. - Concluded.

compressor discharge pressure and temperature increase. The turbine inlet temperature reaches 820 K (1475° R) and then rises to the final value of 1078.3 K (1941° R) as the engine accelerates to 100 percent corrected speed.

Effect of Cruise Altitude on Fuel Control Performance

The simulation results were used to predict the effects of various fuel controls on flight dynamics of a missile having a nominal drag force of 1557 newtons (350 lbf) at a

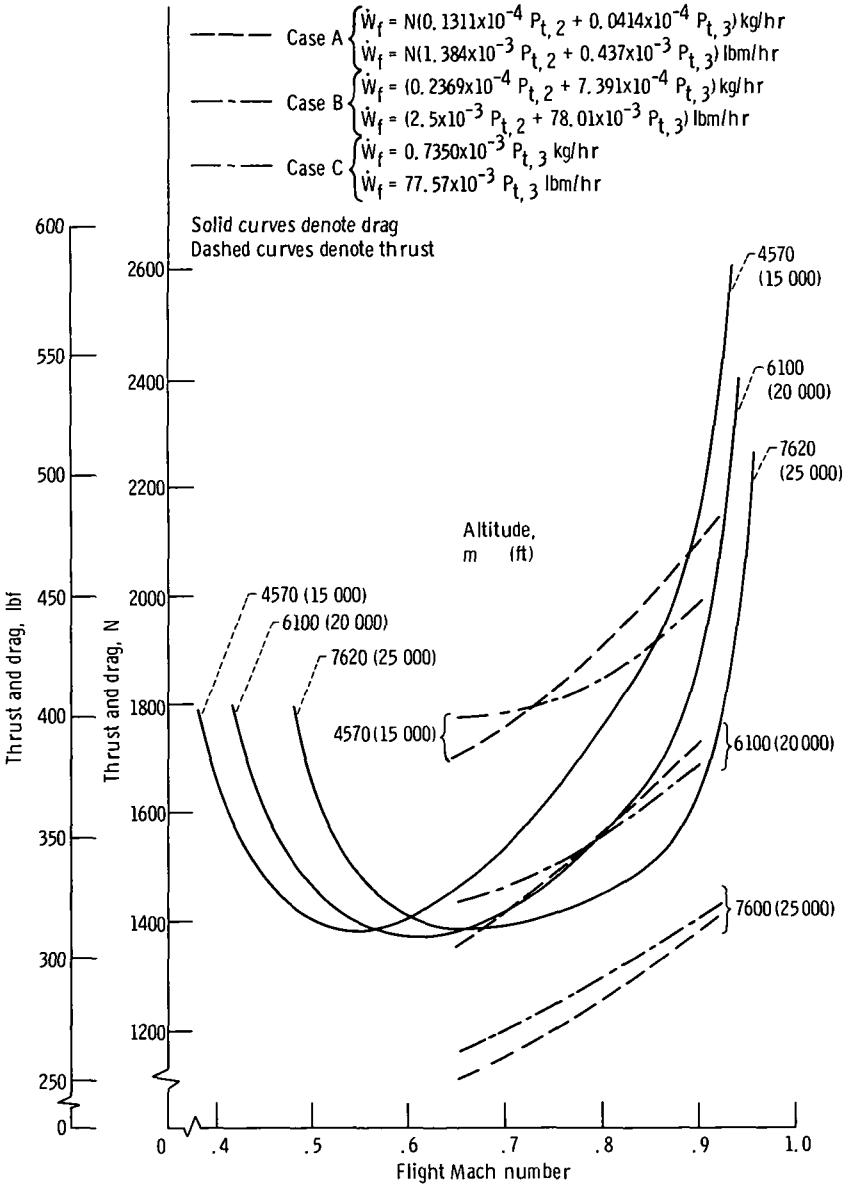

Figure 16. - Engine, control, and vehicle flight dynamics.

Mach number of 0.8 and an altitude of 6100 meters (20 000 ft). The engine and fuel control are designed to produce 1557 newtons (350 lbf) thrust at this flight condition.

Figure 16 shows the variation of thrust and drag with Mach number for altitudes of 4570, 6100, and 7620 meters (15 000, 20 000, and 25 000 ft, respectively). The thrust plotted is that which would result from the use of the fuel control calibrated to give 1557 newtons (350 lbf) nominal thrust at the nominal cruise condition of Mach 0.8 at 6100 meters (20 000 ft) altitude. Drag is assumed to be typical of a missile designed to cruise at this flight condition.

CONCLUSIONS

The computer analysis of the drone engine indicates that the engine performance is satisfactory over the desired flight range. It is shown that sufficient stall margin is available to accelerate the engine from windmilling to design speed.

The fuel schedules A, B, and C will accelerate the engine over the specified range of flight conditions to design speed. The generalized parameter control provides satisfactory performance over the desired flight range of the engine. This type of control is recommended for the drone application.

Lewis Research Center,
National Aeronautics and Space Administration,
Cleveland, Ohio, January 13, 1972,
132-15.

APPENDIX A

SYMBOLS

A	area, m^2; ft^2
b	coefficient, kg/hr; lbm/hr
C_A	coefficient
C_n	coefficients, $(rpm)^2/(K)^2$; $(rpm)^2/(^oR)^2$
C_p	specific heat at constant pressure, J/(kg)(K); Btu/(lbm)(^oR)
E	energy, N-m/sec; ft-lbf/sec
g	gravitational constant, 1 (kg)(m)/(N)(sec^2); 32.17 (lbm)(ft)/(lbf)(sec^2)
h	enthalpy, J/kg; Btu/lbm
Δh	enthalpy drop, J/kg; Btu/lbm
I	inertia of rotating mass, N-m-sec^2; lbf-ft-sec^2
J	mechanical equivalent of heat, 1 N-m/J; 778.3 ft-lbf/Btu
K_n	coefficient, (rpm)(sec)/m; (rpm)(sec)/ft
k	coefficient, $(N^2)(sec^2)/(kg^2)(m^4)(K)$; $(lbf^2)(sec^2)/(lbm^2)(ft^4)(^oR)$
k_A	coefficient, $(N)(sec)/(kg)(K)^{1/2}(m)^2$; $(lbf)(sec)/(lbm)(^oR)^{1/2}(ft)^2$
L_C	compressor torque, N-m; ft-lbf
L_T	turbine torque, N-m; ft-lbf
l	length, m; ft
M	Mach number
N	rotational speed, rpm
P	pressure, N/m^2; lbf/ft^2
R	universal gas constant, 287 (N)(m)/(kg)(K); 53.3 (lbf)(ft)/(lbm)(^oR)
r	mean radius, m; ft
r_T	tip radius, m; ft
s	Laplace operator, sec^{-1}
T	temperature, K; ^oR
t	time, sec

U_m mean rotor speed, m/sec; ft/sec

V volume, m^3; ft^3

v_z axial velocity, m/sec; ft/sec

$\dot{W}$ weight flow, kg/sec; lbm/sec

$\dot{W}_f''$ externally acted upon fuel flow, kg/sec; lbm/sec

α coefficient, 30 sec/min

β rotor air inlet angle, deg

γ ratio of specific heats, 1.4

δ ratio of total pressure to standard atmospheric pressure

η efficiency

θ ratio of total temperature to sea-level atmospheric temperature

ρ weight density, kg/m^3; lbm/ft^3

φ flow coefficient

ψ^P pressure coefficient

ψ^T temperature coefficient

Subscripts:

a actual

c variable associated with stage characteristics

d design conditions

f fuel

i ideal

n stage number designation

t total condition

tr total condition reference state

tv total condition variable associated with stage volume

v variable associated with the stage volume

0 free-stream condition

2 compressor inlet

3 compressor discharge

4 combustor

5 turbine

8 nozzle

APPENDIX B

ENGINE SYSTEM SIMULATION - ANALOG REPRESENTATION

The analog computer representation of the drone engine is based on the engine simulation techniques presented in references 1 and 2. The basic simulation consists of representations of the engine components and their associated gas dynamics. The component representations are interconnected to form the complete engine system model.

Compressor Simulation

The modeling techniques used to represent the four-stage axial compressor are based primarily on the method developed in reference 1. Each stage is modeled with steady-state stage characteristics and the gas dynamics of an associated stage volume. The steady-state performance of the individual compressor stages is represented by pressure and temperature rise coefficients ψ_c^P and ψ_c^T which are functions of a flow coefficient φ. These coefficients are mathematically defined for the n^{th} stage as

$$\psi_{c,n}^{P} = \frac{C_n T_{tv,n-1}}{N^2}\left[\left(\frac{P_{tc,n}}{P_{tv,n-1}}\right)^{2/7} - 1\right] \tag{B1}$$

$$\psi_{c,n}^{T} = \frac{C_n}{N^2}\left(T_{tc,n} - T_{tv,n-1}\right) \tag{B2}$$

$$\varphi_{c,n} = \frac{K_n}{N} v_{zc,n} \tag{B3}$$

where

$$C_n = \frac{2gJC_p(\alpha)^2}{\pi^2 r_{T,n}^2}$$

$$K_n = \frac{\alpha}{\pi r_n}$$

Figure 17 presents plots of the pressure and temperature coefficients ψ_c^P and ψ_c^T as functions of the flow coefficient φ, for the four stages of the engine of this report.

The flow coefficient φ is proportional to the ratio of the axial flow velocity and the rotor speed N. The axial-flow velocity can be related to corrected weight flow by

$$\frac{\dot{W}_{c,n}\sqrt{\theta_{v,n-1}}}{\delta_{v,n-1}A_{c,n}} = \frac{v_{zc,n}}{\sqrt{\theta_{v,n-1}}}\left[1 - \left(\frac{v_{zc,n}}{\sqrt{\theta_{v,n-1}}}\right)^2 \frac{1}{2gJC_pT_{tr}\cos^2\beta_n}\right]^{5/2} \rho_{tr} \qquad \text{(B4)}$$

The angle β, defined as the angle between the air velocity vector and the axial direction, was assumed small for the engine system considered. In the actual computer model, the complexities of equation (B4) were avoided by the use of a quadratic fit to a numerical evaluation of the equation. The steady-state representation of the compressor was thus based on the pressure and temperature rise coefficients of figure 17 and the approximation of equation (B4).

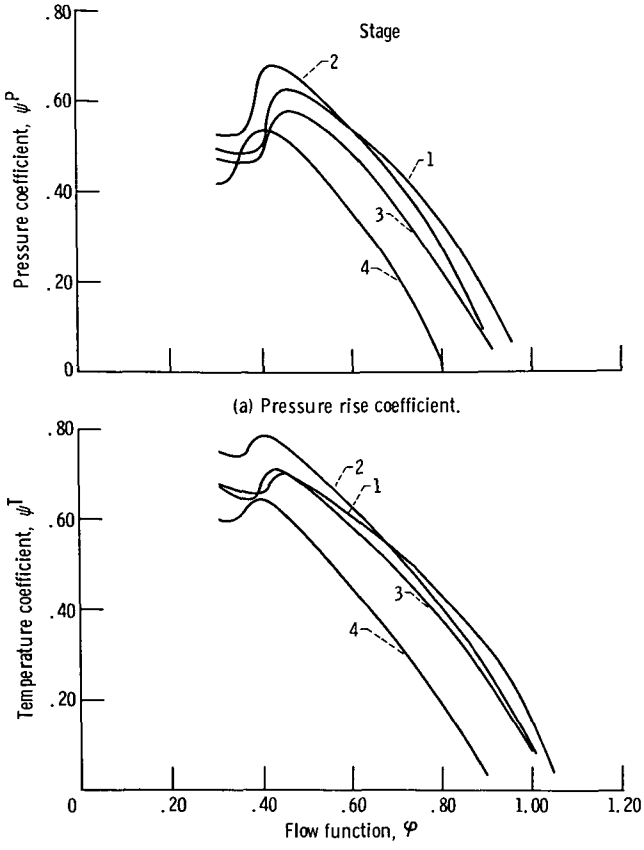

(a) Pressure rise coefficient.

(b) Temperature rise coefficients.

Figure 17. - Compressor stage characteristics.

The gas dynamics for each compressor stage were assumed to occur in an equivalent stage volume conceptually located just downstream of the stage pressure and temperature rise characteristics. The stage dynamics were represented by the following continuity, energy, and momentum balances across the equivalent stage volume:

$$\frac{1}{dt}(\rho_{sv,n}) = \frac{1}{V_n}(\dot{W}_{c,n} - \dot{W}_{c,n+1}) \tag{B5}$$

$$\frac{d}{dt}(\rho_{sv,n}T_{tv,n}) = \frac{\gamma}{V_n}(T_{tc,n}\dot{W}_{c,n} - T_{tv,n}\dot{W}_{c,n+1}) \tag{B6}$$

$$\frac{d}{dt}(\dot{W}_{c,n}) \cong \frac{Ag}{l_r}(P_{tc,n} - P_{tv,n}) \tag{B7}$$

To compute the total pressure in the equivalent stage volume, an equation of state of the following form was assumed:

$$P_{tv,n} \cong R(\rho_{sv,n}T_{tv,n}) \tag{B8}$$

The stage characteristics, the continuity, energy and momentum balance equations, and the equation of state form a complete set for a single compressor stage. Figure 18 presents a block diagram illustrating the computational sequence used for a typical stage. The stage inlet pressure, temperature, and flow are combined to determine the

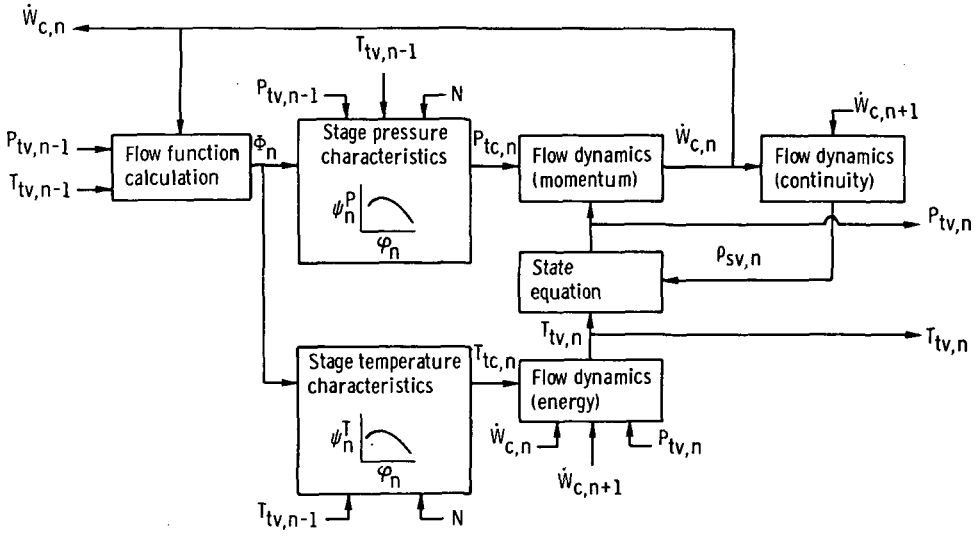

Figure 18. - Block diagram of simulation for n^{th} compressor stage.

flow coefficient φ. The flow coefficient is then used to determine the stage pressure and temperature rise coefficients, and thus the discharge total pressure and temperature. The discharge conditions from the stage maps and the lumped volume gas dynamics are used to compute the conditions in the stage volume, and hence the inlet conditions for the succeeding stage. The overall representation for the complete four-stage compressor was formed by interconnecting the individual stage models.

Combustor Simulation

The combustor simulation was based on a lumped parameter representation of the system gas dynamics and a steady-state map for the efficiency of the combustion process. The combustion efficiency was assumed to be the nonlinear function of pressure and temperature rise presented in figure 19. The simulation did not include combustor blowout limits.

Momentum, continuity, and energy balances were used to represent the system lumped parameter gas dynamics. A detailed discussion of the combustor equations and

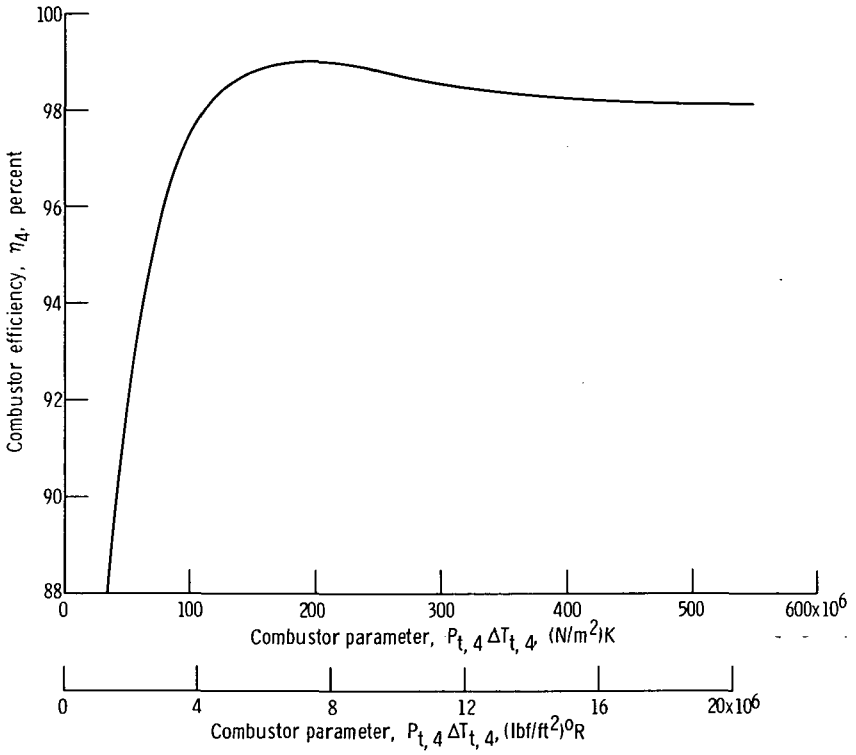

Figure 19. - Combustor efficiency representation.

simulation techniques is presented in reference 2. The pressure drop across the burner was determined from

$$\Delta P'_4 = k \frac{\dot{W}_4^2 T_{t,3}}{P_{t,3}} \tag{B9}$$

and assumed to be 5 percent of the compressor discharge pressure at the design point.

The combustion process itself includes some delays. The combustion delays were included in the simulation by arbitrarily adding a delay of the following form between commanded fuel flow and the fuel flow supplied to the combustor:

$$\frac{\dot{W}''_f}{\dot{W}_f} = \frac{e^{-0.005\ s}}{(1 + 0.003\ s)} \tag{B10}$$

Turbine Simulation

The steady-state representation of the single-stage turbine was based on the curves of figures 20 and 21. The efficiency curve of the first figure was mechanized directly

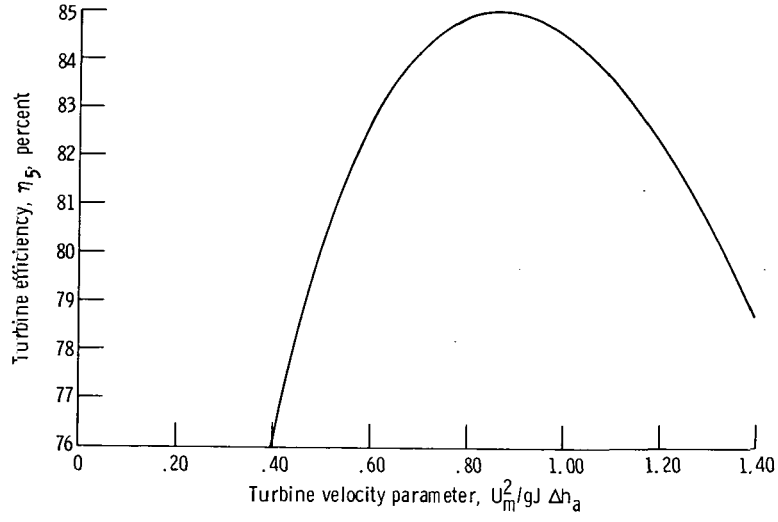

Figure 20. - Turbine efficiency.

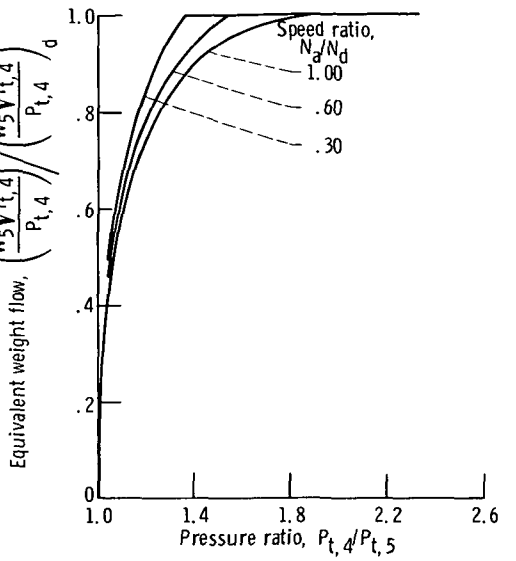

Figure 21. - Turbine flow characteristics.

on a computer function generator, while the more complex flow to pressure ratio relation of the second figure was approximated by

$$\frac{\dot{W}_5\sqrt{T_{t,4}}}{P_{t,4}} = k_A C_A \left[\frac{P_{t,s}}{P_{t,4}}\left(1 - \frac{P_{t,5}}{P_{t,4}}\right)\right]^{1/2} \tag{B11}$$

where

$$C_A = 2.524 - 1.011\frac{N/\sqrt{T_{t,4}}}{\left(N/\sqrt{T_{t,4}}\right)_d} + 0.487\left[\frac{N/\sqrt{T_{t,4}}}{\left(N/\sqrt{T_{t,4}}\right)_d}\right]^2$$

The turbine efficiency characteristic is given as a function of rotor speed and actual enthalpy drop across the turbine. Functionally the relation can be described by

$$\eta_5 = f\left(\frac{U_m^2}{gJ\,\Delta h_a}\right) \tag{B12}$$

where

$$U_m = \frac{\pi r_m N}{\alpha}$$

In the computational sequence, the actual enthalpy drop is assumed and then used to determine the turbine efficiency from the map of equation (B12). The actual enthalpy is also used to determine the turbine discharge temperature T_5 from

$$(T_{t,4} - T_{t,5}) = \frac{1}{C_p} \Delta h_a \tag{B13}$$

The discharge temperature is then used in a continuity balance, across the volume just

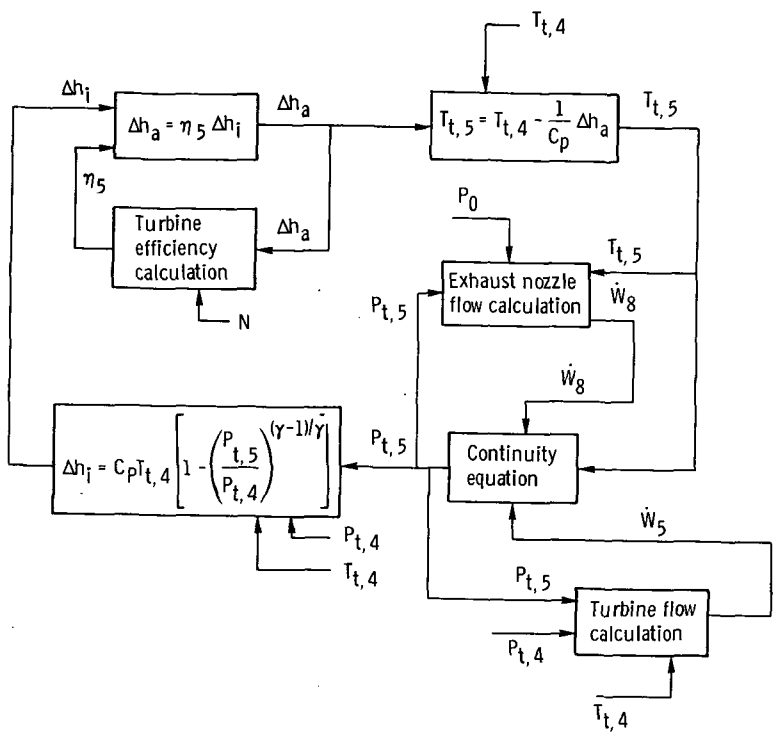

Figure 22. - Computational diagram for turbine.

downstream of the turbine, to compute the discharge pressure. In equation form, this is

$$P_{t,5} = \frac{RT_{t,5}}{V_5} \int (\dot{W}_5 - \dot{W}_8) dt \tag{B14}$$

The discharge pressure is in turn combined with turbine inlet conditions to compute the ideal enthalpy drop from

$$\Delta h_i = C_p T_{t,4} \left[1 - \left(\frac{P_{t,5}}{P_{t,4}} \right)^{(\gamma-1)/\gamma} \right] \tag{B15}$$

The ideal enthalpy drop is multiplied by the efficiency to determine the actual drop assumed earlier in the computational sequence. The calculations are shown in schematic form in figure 22.

Exhaust Nozzle Simulation

The engine exhaust nozzle, located just downstream of the turbine exhaust, was the final engine element included in the simulation. Flow through the fixed area nozzle was computed from

$$\left.\begin{aligned} \frac{\dot{W}_8 \sqrt{T_{t,5}}}{A_8 P_{t,5}} &= \sqrt{\frac{2\gamma g}{R(\gamma - 1)}} \left(\frac{P_0}{P_{t,5}} \right)^{1/\gamma} \left[1 - \left(\frac{P_0}{P_{t,5}} \right)^{(\gamma-1)/\gamma} \right]^{1/2}, \quad 0.530 \leq \left(\frac{P_0}{P_{t,5}} \right) \leq 1.0 \\ \frac{\dot{W}_8 \sqrt{T_{t,5}}}{A_8 P_{t,5}} &= \sqrt{\frac{\gamma g}{R} \left(\frac{2}{\gamma + 1} \right)^{(\gamma+1)/(\gamma-1)}}, \quad 0 \leq \left(\frac{P_0}{P_{t,5}} \right) \leq 0.530 \end{aligned}\right\} \tag{B16}$$

Rotor Dynamics Simulation

The engine rotational speed is determined by integrating a torque balance across the compressor and turbine

$$\frac{dN}{dt} = \frac{30}{\pi I} \sum L \tag{B17}$$

The power required by the compressor can be computed from

$$E = J(\dot{W}_2 C_p T_{t,2} - \dot{W}_3 C_p T_{t,3}) \tag{B18}$$

which results in a torque of

$$L_C = \frac{30J}{\pi N} (\dot{W}_2 C_p T_{t,2} - \dot{W}_3 C_p T_{t,3}) \tag{B19}$$

Similarly, the turbine torque is computed from

$$L_T = \frac{30J}{\pi N} (\dot{W}_5 h_4 - \dot{W}_8 h_5) \tag{B20}$$

and the engine speed equation then becomes

$$\frac{dN}{dt} = \left(\frac{30}{\pi I}\right)(L_C + L_T) \tag{B21}$$

where I is the mass polar moment of inertia of the rotor assembly.

The various component representations were interconnected to form the engine system simulation. The system simulation was then used to investigate and define engine operating characteristics.

APPENDIX C

ENGINE SYSTEM SIMULATION - DIGITAL REPRESENTATION

The digital program uses the system equations to calculate steady-state solutions at various percentages of design speed.

The simulation includes: the four-stage compressor, the burner, the turbine, and the nozzle. The MAIN program calls subroutines which may be classified into three groups: the input-output subroutines, the system subroutines, and the data handling subroutines.

Input-Output Subroutines

INPUT sets constants used in other subroutines

OUTPUT prints desired variables

System Subroutines

CMPRSR solves compressor equations for each stage

BURNER calculates burner variables

TURBIN calculates turbine variables

NOZZLE calculates nozzle variables

Data-Handling Subroutines

TERP1 two-dimensional interpolation for table lookups

TERP2 three-dimensional interpolation for table lookups

BLDATA block data subroutine, includes all necessary data for table lookup

INPUT sets in the area constant for the nozzle, ambient pressure, temperature, specific heat of compressor and burner, gamma of compressor and burner, and various physical constants. Mach number is also calculated but never used.

CMPRSR is entered with weight flow (estimated), pressure, temperature, speed, and geometric and physical constants. It calculates the outlet pressure and temperature

(using phi, psi, and psi prime maps), efficiency, change in enthalpy, and outlet weight flow for each stage. The final calculations are the overall efficiency of the compressor and the sum of the enthalpy changes of the four stages of the compressor.

BURNER is entered with the weight flow, pressure and temperature of the compressor exit, the estimated outlet temperature, and various constants. The enthalpy and the outlet pressure are calculated. The product of the outlet pressure and the delta temperature is calculated and is used in a table lookup to find efficiency. Fuel flow is then calculated.

TURBIN is entered with the weight flow, pressure and temperature (estimated) of the burner exit, compressor speed, fuel flow, the torque of the compressor, and various constants. A table lookup is used to find the efficiency, and from that the outlet pressure and temperature are calculated.

NOZZLE is entered with weight flow, pressure and temperature of the turbine exit, and various constants. Nozzle weight flow, outlet pressure and temperature, and nozzle exit weight flow are calculated.

OUTPUT calculates compressor pressure ratio, corrected weight flow, and corrected speed. It then prints all variables of interest.

TERP1 is a function subprogram which performs two-dimensional interpolation.

TERP2 is a function subprogram which performs three-dimensional interpolation.

BLDATA is a block data subroutine which contains data for table lookups of psi, psi prime, phi, tip radii, mean radii, areas, $P_{t,4}\,\Delta T$, burner efficiency, $N/\sqrt{T_{t,4}}$, $P_{t,4}/P_{t,5}$, weight flow parameter, turbine enthalpy parameter, and turbine efficiency.

A flow chart for the drone engine is presented in figure 23. The Newton-Raphson method of convergence is used in both the burner temperature iteration and the inlet weight flow iteration.

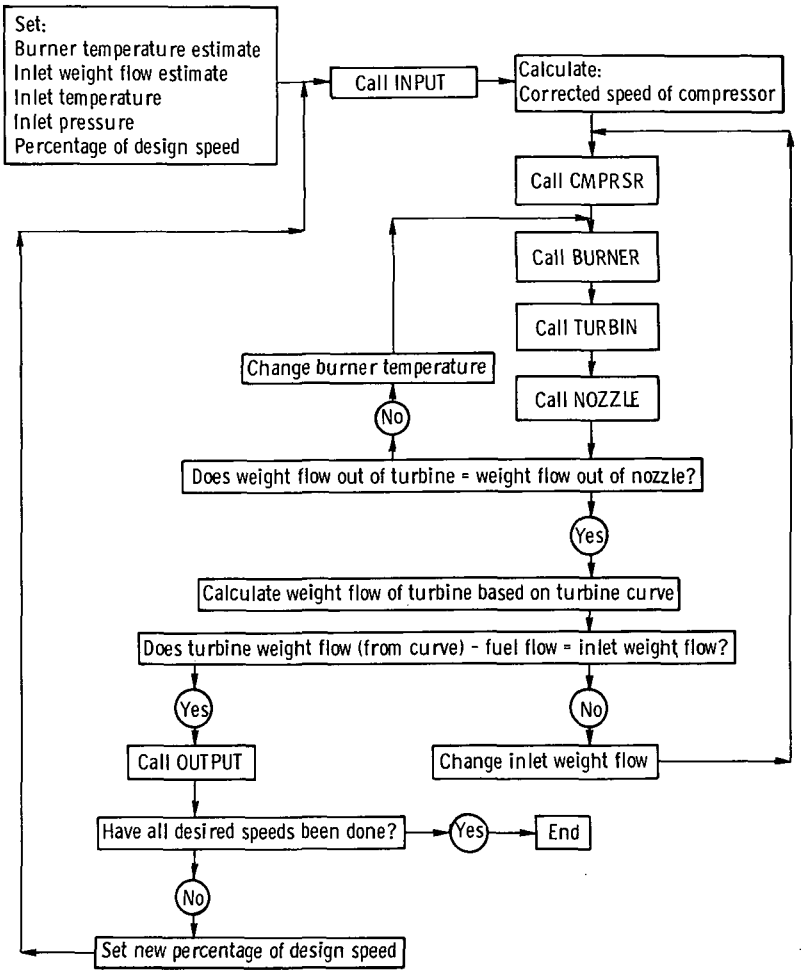

Figure 23. - Flowchart for drone engine.

Digital Computer Program

```
$IBFTC MAIN     LIST
       COMMON  / VAR / N, PI, TI, WI, SUMDHC, ETACOM, THET, T(4), P(4),
      1 W(4), ETAC(4), DELHC(4), PHI(4), PSI(4), PSIP(4), MC(4), WFG,
      2 DHT, ETAT, P3, T3, W3, T4, P4, W4, T5, P5, W5, T6, P6, W6, W7,
      3 ETAB, T4G
       COMMON  / CONST / GAMMA, GAMMA1, GAMMAB, G, CPC, CPB, AJ, RK, R2P,
      1 SCONST, PA, TA, MA, HC, CONST7
       COMMON  / BLOA / XPHI(30,4), YPSI(30,4), YPSIP(30,4), R(4), RM(4),
      1 A(4), SPEED(12), XP4DTB(16), YETAB(16), XP4P5(19), XNT4(3),
      2 YWSRTP(19,3), XUTERM(25), YEFF(25)
       REAL  N, MC, MA, NT4
C
C
C
C      PERCENT OF RADII / 100.0
       GEOMR = 1.0
C      SQUARE ROOT OF PERCENT OF AREA / 100.0
       GEOMA = 1.0
C      PRINT PAGE CONSTANT
       L = 0
       WRITE (6,3)
    3  FORMAT  (1H1)
       DO 2  J = 1,4
       R(J) = GEOMR * R(J)
       RM(J) = GEOMR * RM(J)
    2  A(J) = GEOMA * GEOMA * A(J)
C      INLET FLOW, PRESSURE, AND TEMPERATURE ESTIMATES
       WI = 15.0
       PI = 20.4
       TI =  518.7
C      BURNER TEMPERATURE ESTIMATE
       T4G = 1960.0
       DO 30  K = 1,10
       WI = .93 * WI
       CALL INPUT
       THET = SQRT(TI / 518.7)
       XX = THET * SPEED(K) / 100.0
       N = 35260.0 * XX
       SCONST = 19.7392 * N * N / AJ / G / CPC / 3600.0 / 144.0
       IJCONV = 0
    1  CALL OUTPUT(L)
       CALL CMPRSR
       KCONV = 0
       LGCONV = 0
    5  CALL BURNER
       T4 = T4G
    6  CALL TURBIN
    7  CALL NOZZLE
C      CONVERGENCE OF WEIGHT FLOWS IN TURBINE AND NOZZLE
       ERW = W5 - W7
       IF (ABS(ERW) .LE. .0001 * W5)  GO TO 15
       LGCONV = LGCONV + 1
       IF (LGCONV .LT. 50)  GO TO 36
       WI = .999 * WI
       GO TO 1
```

```
  36  IF (ERW .NE. ERWP)  GO TO 35
      WI = .999 * WI
      GO TO 1
  35  IF (KCONV .GT. 0)  GO TO 10
      T4GP = T4G
      ERWP = ERW
      T4G = .99 * T4G
      KCONV = 1
      GO TO 5
  10  T4GN = (T4G * ERWP - T4GP * ERW) / (ERWP - ERW)
      IF (T4GN .GT. T3)  GO TO 37
      T4G = 1.25 * T3
      WI = 1.001 * WI
      GO TO 1
  37  IF (T4GN .NE. T4G)  GO TO 34
      WI = .999 * WI
      GO TO 1
  34  IF (T4GN .LT. .99 * T4G)  T4GN = .99 * T4G
      IF (T4GN .GT. 1.01 * T4G)  T4GN = 1.01 * T4G
      T4GP = T4G
      ERWP = ERW
      T4G = T4GN
      KCONV = KCONV + 1
      GO TO 5
C     CONVERGENCE OF INLET AND OUTLET WEIGHT FLOWS
  15  NT4 = N / SQRT(T4)
      IF (NT4 .GT. XNT4(1))  GO TO 4
      IXN = 2
      XXN = 0.0
      GO TO 11
   4  DO 9  IXN = 2,3
      IXN = IXN
      IF (NT4 .GE. XNT4(IXN-1) .AND. NT4 .LT. XNT4(IXN))  GO TO 12
   9  CONTINUE
      IXN = 3
      XXN = 1.0
      GO TO 11
  12  XXN = (NT4 - XNT4(INX-1)) / (XNT4(IXN) - XNT4(IXN-1))
  11  P4P5 = P4 / P5
      IF (P4P5 .GT. XP4P5(1))  GO TO 13
      IXP = 2
      XXP = 0.0
      GO TO 17
  13  DO 14  IXP = 2,19
      IXP = IXP
      IF (P4P5 .GE. XP4P5(IXP-1) .AND. P4P5 .LT. XP4P5(IXP))  GO TO 16
  14  CONTINUE
      IXP = 19
      XXP = 1.0
      GO TO 17
  16  XXP = (P4P5 - XP4P5(IXP-1)) / (XP4P5(IXP) - XP4P5(IXP-1))
  17  W5RTP = TERP2(XXP, XXN, YW5RTP(IXP,IXN), YW5RTP(IXP-1,IXN),
     1 YW5RTP(IXP,IXN-1), YW5RTP(IXP-1,IXN-1))
      W5C = (W5RTP * P4 / SQRT(T4))
      WOUT = W5C - WFG
      IF (ABS(WI - WOUT) .LE. .0001 * ABS(WI))  GO TO 25
      IF (IJCONV .GT. 0)  GO TO 20
      WIP = WI
      WOUTP = WOUT
```

```
      WI = 1.005 * WI
      IJCONV = 1
      GO TO 1
   20 WIN = (WOUTP * WI - WOUT * WIP) / ((WI - WIP) - (WOUT - WOUTP))
      IF (WIN .LT. .994 * WI)  WIN = .994 * WI
      IF (WIN .GT. 1.006 * WI)  WIN = 1.006 * WI
      IF (WIN .GT. WI)  T4G = (WI / WIN) * T4G
      IF (WIN .LT. WI)  T4G = (WIN / WI) * T4G
      WIP = WI
      WOUTP = WOUT
      WI = WIN
      IJCONV = IJCONV + 1
      GO TO 1
   25 CALL OUTPUT(L)
   30 CONTINUE
      RETURN
      END
```

```
$IBFTC INPUT   LIST
      SUBROUTINE  INPUT
      COMMON  / CONST / GAMMA, GAMMA1, GAMMAB, G, CPC, CPB, AJ, RK, R2P,
     1 SCONST, PA, TA, MA, HC, CONST7
      REAL  MA
C
C
C
      CONST7 = 56.3
      MA = .8
      PA = 14.7
      TA = 518.7
      CPC = .24
      CPB = .278
      GAMMA = 1.4
      GAMMAB = 1.34
      G = 32.16
      AJ = 778.12
      RK = 640.32
      GAMMA1 = GAMMA - 1.0
      R2P = RK / 6.2832
      HC = 18640.0
      RETURN
      END
```

```
$IBFTC CMPRSR  LIST
       SUBROUTINE  CMPRSR
       COMMON  / VAR / N, PI, TI, WI, SUMDHC, ETACOM, THET, T(4), P(4),
      1 W(4), ETAC(4), DELHC(4), PHI(4), PSI(4), PSIP(4), MC(4), WFG,
      2 DHT, ETAT, P3, T3, W3, T4, P4, W4, T5, P5, W5, T6, P6, W6, W7,
      3 ETAB, T4G
       COMMON  / CONST / GAMMA, GAMMA1, GAMMAB, G, CPC, CPB, AJ, RK, R2P,
      1 SCONST, PA, TA, MA, HC, CONST7
       COMMON  / BLDA / XPHI(30,4), YPSI(30,4), YPSIP(30,4), R(4), RM(4),
      1 A(4), SPEED(12), XP4DTB(16), YETAB(16), XP4P5(19), XNT4(3),
      2 YWSRTP(19,3), XUTERM(25), YEFF(25)
       REAL  N, MC, MA
C
C
C
C      STAGE 1
       WC = WI * SQRT(RK * TI) / PI / A(1)
       MCONV = 0
       VG = WI * RK * TI / PI / A(1)
    1  RAD = VG * VG / RK / TI * GAMMA1 / 24.0 / G / GAMMA
       IF (RAD .LE. 1.0)  GO TO 6
       WI = 100.0 * WI
       RETURN
    6  WTERM = VG / SQRT(RK * TI) * ((1.0 - RAD) ** (1.0 / GAMMA1))
       ERW = WC - WTERM
       IF (ABS(ERW) .LE. .000001 * ABS(WC))  GO TO 3
       IF (MCONV .GT. 0)  GO TO 2
       VGP = VG
       ERWP = ERW
       VG = .99 * VG
       MCONV = 1
       GO TO 1
    2  VGN = (VG * ERWP - VGP * ERW) / (ERWP - ERW)
       VGP = VG
       ERWP = ERW
       VG = VGN
       MCONV = MCONV + 1
       GO TO 1
    3  PHI(1) = 60.0 * VG / 6.2832 / RM(1) / N
       IF (PHI(1) .GT. XPHI(1,1))  GO TO 4
       IX = 2
       GO TO 10
    4  DO 5  IX = 2,30
       IX = IX
       IF (PHI(1) .GE. XPHI(IX-1,1) .AND. PHI(1) .LT. XPHI(IX,1))
      1 GO TO 10
    5  CONTINUE
       IX = 30
   10  XX = (PHI(1) - XPHI(IX-1,1)) / (XPHI(IX,1) - XPHI(IX-1,1))
   15  PSI(1) = TERP1(XX, YPSI(IX,1), YPSI(IX-1,1))
       IF (PSI(1) .NE. 0.0)  GO TO 103
       DO 101  L = 1,30
       K = 32 - L
       IF (YPSI(K-1,1) .NE. 0.0)  GO TO 102
  101  CONTINUE
  102  XK = (PHI(1) - XPHI(K-1,1)) / (XPHI(IX,1) - XPHI(K-1,1))
       PSI(1) = TERP1(XK, YPSI(K,1), YPSI(K-1,1))
  103  PSIP(1) = TERP1(XX, YPSIP(IX,1), YPSIP(IX-1,1))
       IF (PSIP(1) .NE. 0.0)  GO TO 106
```

```
      DO 104  L = 1,30
      K = 32 - L
      IF (YPSIP(K-1,1) .NE. 0.0)  GO TO 105
  104 CONTINUE
  105 XK = (PHI(1) - XPHI(K-1,1)) / (XPHI(IX,1) - XPHI(K-1,1))
      PSIP(1) = TERP1(XK, YPSIP(K,1), YPSIP(K-1,1))
  106 ETAC(1) = PSIP(1) / PSI(1)
      MC(1) = SQRT((9.8696 * RM(1) * RM(1) * N * N / TI - VG * VG / TI)
     1 / (21600.0 * G * RK * (1.0 - GAMMA1 * VG * VG / 24.0 / G / RK /
     2 GAMMA / TI)))
      P(1) = PI * ((PSIP(1) * SCONST * R(1) * R(1) / TI + 1.0) **
     1 (GAMMA / GAMMA1))
      T(1) = TI + PSI(1) * SCONST * R(1) * R(1)
      DELPC(1) = WI * CPC * (T(1) - TI)
      W(1) = WI
C     STAGES 2 THROUGH 4
      DO 35  I = 2,4
      W(I) = W(I-1)
      WC = W(I) * SQRT(RK * T(I-1)) / P(I-1) / A(I)
      NCONV = 0
      VG = W(I) * RK * T(I-1) / P(I-1) / A(I)
   16 RAD = VG * VG / RK / T(I-1) * GAMMA1 / 24.0 / G / GAMMA
      IF (RAD .LE. 1.0)  GO TO 36
      WI = 100.0 * WI
      RETURN
   36 WTERM = VG / SQRT(RK * T(I-1)) * ((1.0 - RAD) ** (1.0 / GAMMA1))
      ERW = WC - WTERM
      IF (ABS(ERW) .LE. .000001 * ABS(WC))  GO TO 18
      IF (NCONV .GT. 0)  GO TO 17
      VGP = VG
      ERWP = ERW
      VG = .99 * VG
      NCONV = 1
      GO TO 16
   17 VGN = (VG * ERWP - VGP * ERW) / (ERWP - ERW)
      VGP = VG
      ERWP = ERW
      VG = VGN
      NCONV = NCONV + 1
      GO TO 16
   18 PHI(I) = 60.0 * VG / 6.2832 / RM(I) / N
      IF (PHI(I) .GT. XPHI(1,I))  GO TO 19
      IX = 2
      GO TO 25
   19 DO 20  IX = 2,30
      IX = IX
      IF (PHI(I) .GE. XPHI(IX-1,I) .AND. PHI(I) .LT. XPHI(IX,I))
     1 GO TO 25
   20 CONTINUE
      IX = 30
   25 XX = (PHI(I) - XPHI(IX-1,I)) / (XPHI(IX,I) - XPHI(IX-1,I))
   30 PSI(I) = TERP1(XX, YPSI(IX,I), YPSI(IX-1,I))
      IF (PSI(I) .NE. 0.0)  GO TO 109
      DO 107  L = 1,30
      K = 32 - L
      IF (YPSI(K-1,I) .NE. 0.0)  GO TO 108
  107 CONTINUE
  108 XK = (PHI(I) - XPHI(K-1,I)) / (XPHI(IX,I) - XPHI(K-1,I))
      PSI(I) = TERP1(XK, YPSI(K,I), YPSI(K-1,I))
```

```
109   PSIP(I) = TERP1(XX, YPSIP(IX,I), YPSIP(IX-1,I))
      IF (PSIP(I) .NE. 0.0)  GO TO 32
      DO 110  L = 1,30
      K = 32 - L
      IF (YPSIP(K-1,I) .NE. 0.0)  GO TO 111
110   CONTINUE
111   XK = (PHI(I) - XPHI(K-1,I)) / (XPHI(IX,I) - XPHI(K-1,I))
      PSIP(I) = TERP1(XK, YPSIP(K,I), YPSIP(K-1,I))
 32   ETAC(I) = PSIP(I) / PSI(I)
 33   MC(I) = SQRT((9.8696 * RM(I) * RM(I) * N * N / T(I-1) - VG * VG /
     1 T(I-1)) / (21600.0 * G * RK * (1.0 - GAMMA1 * VG * VG / 24.0 / G
     2 / RK / GAMMA / T(I-1))))
      P(I) = P(I-1) * ((PSIP(I) * SCONST * R(I) * R(I) / T(I-1) + 1.0)
     1 ** (GAMMA / GAMMA1))
      T(I) = T(I-1) + PSI(I) * SCONST * R(I) * R(I)
      DELHC(I) = W(I) * CPC * (T(I) - T(I-1))
 35   CONTINUE
      P3 = P(4)
      T3 = T(4)
      W3 = W(4)
      SUMDHC = 0.0
      DO 40  I = 1,4
 40   SUMDHC = SUMDHC + DELHC(I)
      ETACOM = ((P3 / PI) ** (GAMMA1 / GAMMA) - 1.0) / ((T3 / TI) - 1.0)
      RETURN
      END
```

```
$IBFTC BURNER  LIST
      SUBROUTINE  BURNER
      COMMON  / VAR / N, PI, TI, WI, SUMDHC, ETACOM, THET, T(4), P(4),
     1 W(4), ETAC(4), DELHC(4), PHI(4), PSI(4), PSIP(4), MC(4), WFG,
     2 DHT, ETAT, P3, T3, W3, T4, P4, W4, T5, P5, W5, T6, P6, W6, W7,
     3 ETAB, T4G
      COMMON  / CONST / GAMMA, GAMMA1, GAMMAB, G, CPC, CPB, AJ, RK, R2P,
     1 SCONST, PA, TA, MA, HC, CONST7
      COMMON  / BLDA / XPHI(30,4), YPSI(30,4), YPSIP(30,4), R(4), RM(4),
     1 A(4), SPEED(12), XP4DTB(16), YETAB(16), XP4P5(19), XNT4(3),
     2 YW5RTP(19,3), XUTERM(25), YEFF(25)
      REAL  N, MC, MA
C
C
C
      W4 = W3
   1  P4 = P3 - .00214 * W4 * W4 * T3 / P3
      P4DTB = P4 * (T4G - T3) + 1800.0
      IF (P4DTB .GT. XP4DTB(1))  GO TO 2
      IX = 2
      XX = 0.0
      GO TO 15
   2  DO 5  IX = 2,16
      IX = IX
      IF (P4DTB .GE. XP4DTB(IX-1) .AND. P4DTB .LT. XP4DTB(IX))  GO TO 10
   5  CONTINUE
      IX = 16
      XX = 1.0
      GO TO 15
  10  XX = (P4DTB - XP4DTB(IX-1)) / (XP4DTB(IX) - XP4DTB(IX-1))
  15  ETAB = TERP1(XX, YETAB(IX), YETAB(IX-1)) * .9915
      H4 = T4G * CPB
      WFG = W4 * (CPB * T3 - H4) / (H4 - ETAB * HC)
      RETURN
      END
```

```
$IBFTC TURBIN  LIST
       SUBROUTINE  TURBIN
       COMMON  / VAR / N, PI, TI, WI, SUMDHC, ETACOM, THET, T(4), P(4),
      1 W(4), ETAC(4), DELHC(4), PHI(4), PSI(4), PSIP(4), MC(4), WFG,
      2 DHT, ETAT, P3, T3, W3, T4, P4, W4, T5, P5, W5, T6, P6, W6, W7,
      3 ETAB, T4G
       COMMON  / CONST / GAMMA, GAMMA1, GAMMAB, G, CPC, CPB, AJ, RK, R2P,
      1 SCONST, PA, TA, MA, HC, CONST7
       COMMON  / BLDA / XPHI(30,4), YPSI(30,4), YPSIP(30,4), R(4), RM(4),
      1 A(4), SPEED(12), XP4DTB(16), YETAB(16), XP4P5(19), XNT4(3),
      2 YWSRTP(19,3), XUTERM(25), YEFF(25)
       REAL  N, MC, MA, NT4
C
C
C
       W5 = W4 + WFG
       DHACT = SUMDHC / W5
       DHT = SUMDHC
       U = 8.73E-3 * 3.97 * N
       UT = U * U / G / AJ
       UTERM = UT / DHACT
       IF (UTERM .GT. XUTERM(1))  GO TO 50
       IXU = 2
       XXU = 0.0
       GO TO 65
  50   DO 55  IXU = 2,25
       IXU = IXU
       IF (UTERM .GE. XUTERM(IXU-1) .AND. UTERM .LT. XUTERM(IXU))
      1 GO TO 60
  55   CONTINUE
       IXU = 25
       XXU = 1.0
       GO TO 65
  60   XXU = (UTERM - XUTERM(IXU-1)) / (XUTERM(IXU) - XUTERM(IXU-1))
  65   ETAT = TERP1(XXU, YEFF(IXU), YEFF(IXU-1))
       DHID = DHACT / ETAT
       P5 = P4 * ((1.0 - DHID / CPB / T4G) ** (GAMMAB / (GAMMAB - 1.0)))
       T5 = T4G - DHACT / CPB
       RETURN
       END
```

```
$IBFTC NOZZLE  LIST
      SUBROUTINE  NOZZLE
      COMMON  / VAR / N, PI, TI, WI, SUMDHC, ETACOM, THET, T(4), P(4),
     1 W(4), ETAC(4), DELHC(4), PHI(4), PSI(4), PSIP(4), MC(4), WFG,
     2 DHT, ETAT, P3, T3, W3, T4, P4, W4, T5, P5, W5, T6, P6, W6, W7,
     3 ETAB, T4G
      COMMON  / CONST / GAMMA, GAMMA1, GAMMAB, G, CPC, CPB, AJ, RK, R2P,
     1 SCONST, PA, TA, MA, HC, CONST7
      REAL  N, MC, MA
C
C
C
      W6 = W5
      P6 = P5
      T6 = T5
      PAP6 = PA / P6
      IF (PAP6 .LT. .5283)  PAP6 = .5283
      IF (PAP6 .GT. 1.0)  PAP6 = 1.0
      W7 = CONST7 * P6 * (PAP6 ** (1.0 / GAMMA)) * SQRT(1.0 - (PAP6 **
     1 (GAMMA1 / GAMMA))) / SQRT(T6)
      RETURN
      END
```

```
$IBFTC OUTPUT  LIST
      SUBROUTINE  OUTPUT(L)
      COMMON  / VAR / N, PI, TI, WI, SUMDHC, ETACOM, THET, T(4), P(4),
     1 W(4), ETAC(4), DELHC(4), PHI(4), PSI(4), PSIP(4), MC(4), WFG,
     2 DHT, ETAT, P3, T3, W3, T4, P4, W4, T5, P5, W5, T6, P6, W6, W7,
     3 ETAB, T4G
      REAL  N, MC
C
C
C
      L = L + 1
      POPI = P3 / PI
      CORW = WI * THET / (PI / 14.7)
      CORN = (N / THET / 35260.0) * 100.0
      WRITE (6,10)  N, WFG, PI, TI, WI, P(1), T(1), W(1), ETAC(1),
     2 DELHC(1), P(2), T(2), W(2), ETAC(2), DELHC(2), P(3), T(3), W(3),
     3 ETAC(3), DELHC(3), P(4), T(4), W(4), ETAC(4), DELHC(4), P3, T3,
     4 W3, ETACOM, SUMDHC, P4, T4, W4, ETAB, P5, T5, W5, ETAT, DHT, P6,
     5 T6, W6, W7, POPI, CORW, CORN
  10  FORMAT  (1HO, 9HN       = , 1PE14.6, 10X, 9HWFG     = , 1PE14.6 /
     1 1X, 7HSTATION, 16X, 8HPRESSURE, 17X, 4HTEMP, 21X, 1HW, 22X,
     2 3HEFF, 21X, 2HDH / 1X, 5HINLET, 4X, 1P3E24.6 / 1X, 6HCOMP 1, 3X,
     3 1P5E24.6 / 1X, 6HCOMP 2, 3X, 1P5E24.6 / 1X, 6HCOMP 3, 3X,
     4 1P5E24.6 / 1X, 6HCOMP 4, 3X, 1P5E24.6 / 1X, 9HCOMP EXIT, 1P5E24.6
     5 / 1X, 6HBURNER, 3X, 1P4E24.6 / 1X, 7HTURBINE, 2X, 1P5E24.6 / 1X,
     6 6HNOZZLE, 3X, 1P3E24.6 / 1X, 8HNOZ EXIT, 49X, 1PE24.6 / 1X,
     7 7HPOPI = , 1PE14.6, 10X, 11HCORR W    = , 1PE14.6, 10X, 12HPERCENT
     8 N = , 1PE14.6)
      WRITE (6,20)  (PHI(I), PSI(I), PSIP(I), MC(I),  I = 1,4)
  20  FORMAT  (23X, 3HPHI, 21X, 3HPSI, 21X, 4HPSIP, 15X,
     1 13HINLET MACH NO / 1X, 6HCOMP 1, 1P4E24.6 / 1X, 6HCOMP 2,
     2 1P4E24.6 / 1X, 6HCOMP 3, 1P4E24.6 / 1X, 6HCOMP 4, 1P4E24.6)
      IF (L .LT. 3)  RETURN
      WRITE (6,30)
  30  FORMAT  (1H1)
      L = 0
      RETURN
      END
```

```
$IBFTC TERP1   LIST
      FUNCTION  TERP1  (X, A, B)
C
C
C
      TERP1 = B + (A - B) * X
      RETURN
      END
```

```
$IBFTC TERP2   LIST
      FUNCTION  TERP2  (X, Y, A, B, C, D)
C
C
C
      TERP2 = D + (B - D) * Y + (C - D) * X - (C + B - A - D) * X * Y
      RETURN
      END



$IBFTC BLDATA  LIST
      BLOCK DATA
      COMMON  / BLDA / XPHI(30,4), YPSI(30,4), YPSIP(30,4), R(4), RM(4),
     1 A(4), SPEED(12), XP4DTB(16), YETAB(16), XP4P5(19), XNT4(3),
     2 YW5RTP(19,3), XUTERM(25), YEFF(25)
C
C
C
C     PSI DATA
      DATA  ((YPSI(I,K),  I = 1,30),  K = 1,4) /
C     PSI PRIME DATA
      DATA  ((YPSIP(I,K),  I = 1,30),  K = 1,4) /
C     PHI DATA
      DATA  ((XPHI(I,K),  I = 1,30),  K = 1,4) /
C     TIP RADII DATA
      DATA  R /
C     MEAN RADII DATA
      DATA  RM /
C     STAGE AREAS DATA
      DATA  A /
C     DESIRED PERCENTAGES OF DESIGN MECHANICAL SPEED
      DATA  SPEED /
C     P4DELTA T PARAMETER DATA
      DATA  XP4DTB /
C     BURNER EFFICIENCY DATA
      DATA  YETAB /
C     N/T4 PARAMETER DATA
      DATA  XNT4 /
C     P4/P5 PARAMETER DATA
      DATA  XP4P5 /
C     TURBINE WEIGHT FLOW PARAMETER DATA
      DATA  ((YW5RTP(I,J),  I = 1,19),  J = 1,3)  /
C     TURBINE TORQUE PARAMETER DATA
      DATA  XUTERM /
C     TURBINE EFFICIENCY DATA
      DATA  YEFF /
      END
```

REFERENCES

1. Willoh, Ross G.; and Seldner, Kurt: Multistage Compressor Simulation Applied to the Prediction of Axial Flow Instabilities. NASA TM X-1880, 1969.

2. Seldner, Kurt; Mihaloew, James R.; and Blaha, Ronald J.: Generalized Simulation Technique for Turbojet Engine System Analysis. NASA TN D-6610, 1971.

3. Vanco, Michael R.: Computer Program for Design-Point Performance of Turbojet and Turbofan Engine Cycles. NASA TM X-1340, 1967.

4. Seldner, Kurt; and Gold, Harold: Computer and Engine Performance Study of a Generalized Parameter Fuel Control for Jet Engines. NASA TN D-5871, 1970.

NASA-Langley, 1972 —— 28 E-6688

"The aeronautical and space activities of the United States shall be conducted so as to contribute . . . to the expansion of human knowledge of phenomena in the atmosphere and space. The Administration shall provide for the widest practicable and appropriate dissemination of information concerning its activities and the results thereof."

—NATIONAL AERONAUTICS AND SPACE ACT OF 1958

NASA SCIENTIFIC AND TECHNICAL PUBLICATIONS

TECHNICAL REPORTS: Scientific and technical information considered important, complete, and a lasting contribution to existing knowledge.

TECHNICAL NOTES: Information less broad in scope but nevertheless of importance as a contribution to existing knowledge.

TECHNICAL MEMORANDUMS: Information receiving limited distribution because of preliminary data, security classification, or other reasons.

CONTRACTOR REPORTS: Scientific and technical information generated under a NASA contract or grant and considered an important contribution to existing knowledge.

TECHNICAL TRANSLATIONS: Information published in a foreign language considered to merit NASA distribution in English.

SPECIAL PUBLICATIONS: Information derived from or of value to NASA activities. Publications include conference proceedings, monographs, data compilations, handbooks, sourcebooks, and special bibliographies.

TECHNOLOGY UTILIZATION PUBLICATIONS: Information on technology used by NASA that may be of particular interest in commercial and other non-aerospace applications. Publications include Tech Briefs, Technology Utilization Reports and Technology Surveys.

Details on the availability of these publications may be obtained from:

SCIENTIFIC AND TECHNICAL INFORMATION OFFICE

NATIONAL AERONAUTICS AND SPACE ADMINISTRATION

Washington, D.C. 20546